Improved representation of plant physiology in the JULES-vn5.6 land surface model: Photosynthesis, stomatal conductance and thermal acclimation

Rebecca J. Oliver[1], Lina M. Mercado[1,2], Doug B. Clark[1], Chris Huntingford[1], Christopher M. Taylor[1,5], Pier Luigi Vidale[3], Patrick C. McGuire[3], Markus Todt[3], Sonja Folwell[1], Valiyaveetil Shamsudheen Semeena[1], Belinda E. Medlyn[4]

[1] UK Centre for Ecology and Hydrology, Wallingford, OX10 8BB, UK

[2] College of Life and Environmental Sciences, University of Exeter, Exeter, EX4 4RJ, UK

[3] Department of Meteorology and National Centre for Atmospheric Science, Reading University, Reading RG6 6BB, UK

[4] Hawkesbury Institute for the Environment, Western Sydney University, Australia

[5] National Centre for Earth Observation, Wallingford, OX10 8BB, UK

Journal: GMD – Development and technical paper

Correspondence to: R. J. Oliver (rfu@ceh.ac.uk)

29 **Abstract.**

30 Carbon and water cycle dynamics of vegetation are controlled primarily by photosynthesis and stomatal

31 conductance (g_s). Our goal is to improve the representation of these key physiological processes within the JULES

32 land surface model, with a particular focus on refining the temperature sensitivity of photosynthesis, impacting

33 modelled carbon, energy and water fluxes. We test (1) an implementation of the Farquhar et al. (1980)

34 photosynthesis scheme and associated plant functional type-dependent photosynthetic temperature response

35 functions, (2) the optimality-based g_s scheme from Medlyn et al. (2011), and (3) the Kattge and Knorr (2007)

36 photosynthetic capacity thermal acclimation scheme. New parameters for each model configuration are adopted

37 from recent large observational datasets that synthesise global experimental data. These developments to JULES

38 incorporate current physiological understanding of vegetation behaviour into the model, and enable users to derive

39 direct links between model parameters and on-going measurement campaigns that refine such parameter values.

40 Replacement of the original Collatz *et al.* (1991) C_3 photosynthesis model with the Farquhar scheme results in

41 large changes in GPP for current-day, with ~10% reduction in seasonal (June-August; JJA and December-

42 February; DJF) mean GPP in tropical forests, and ~20% increase in the northern high latitude forests in JJA. The

43 optimality-based g_s model decreases the latent heat flux for the present-day (~10%, with an associated increase in

44 sensible heat flux) across regions dominated by needleleaf evergreen forest in the northern hemisphere summer.

45 Thermal acclimation of photosynthesis coupled with the Medlyn g_s scheme reduced tropical forest GPP by up to

46 5%, and increased GPP in the high northern latitude forests by between 2 to 5%. Evaluation of simulated carbon

47 and water fluxes by each model configuration against global data products show this latter configuration generates

48 improvements in these key areas. Thermal acclimation of photosynthesis coupled with the Medlyn g_s scheme

49 improved modelled carbon fluxes in tropical and high northern latitude forests in JJA, and improved the simulation

50 of evapotranspiration across much of the northern hemisphere in JJA. Having established good model

51 performance for the contemporary period, we force this new version of JULES offline with a future climate

52 scenario corresponding to rising atmospheric greenhouse gases (SSP5 RCP8.5). In particular, these calculations

53 allow understanding of the effects of long-term warming. We find that the impact of thermal acclimation coupled

54 with the optimality-based g_s model on simulated fluxes increases latent heat flux (+50%) by year 2050 compared

55 to the JULES model configuration without acclimation. This new JULES configuration also projects increased

56 GPP across tropical (+10%) and northern latitude regions (+30%) by 2050. We conclude that thermal acclimation

57 of photosynthesis with the Farquhar photosynthesis scheme and the new optimality-based g_s scheme together

58 improve the simulation of carbon and water fluxes for current-day, and has a large impact on modelled future

59 carbon cycle dynamics in a warming world.

60

61

62

63

64

1. Introduction

Photosynthesis and stomatal conductance (g_s) together exert a strong control over the exchange of carbon, water and energy between the land surface and the atmosphere. The behaviour of stomatal pores on the leaf surface link these processes, controlling the amount of carbon dioxide (CO_2) entering, and water leaving each leaf. Photosynthesis represents the largest exchange of carbon between the land and atmosphere (Friedlingstein et al., 2020), being more substantial than respiration loss. This imbalance is central to the global carbon cycle because it slows the rate of accumulation of CO_2 in the atmosphere caused by fossil fuel burning, and therefore also lowers the rate of atmospheric temperature increase. As stomata open to take up CO_2 for photosynthesis, plants also lose water through transpiration, and this flux has been estimated to account for 60–80% of evapotranspiration (ET) across the land surface (Jasechko et al., 2013; Schlesinger and Jasechko, 2014). Hence, for vegetated surfaces, transpiration is the primary driver of the latent heat flux (LE), the latter describing the overall transfer of water vapour to the atmosphere. The partitioning of available net radiation between LE and sensible heat (H) is also a key determinant of land surface temperature, therefore having a feedback on photosynthesis and other key metabolic processes that influence the global carbon cycle such as plant respiration.

Land surface models (LSMs) simulate the exchange of carbon, water and energy between the land surface and the atmosphere, providing the lower boundary conditions for the atmospheric component of Earth System Models (ESMs) when run in a coupled configuration. ESM projections form the main tool to predict future climate change and underpin much of the regular United Nations Intergovernmental Panel on Climate Change (IPCC) reports that inform policymakers. However, ESM predictions of the global carbon sink are fraught with large uncertainties surrounding projections of future carbon uptake (Friedlingstein et al., 2014), causing uncertainty in any translation from CO_2 emissions to atmospheric CO_2 trajectory. A lack of knowledge in how the global carbon cycle operates creates uncertainties in translating from emissions to global warming, and these uncertainties are a sizeable fraction of those associated with unknowns of physical climate processes (Huntingford et al., 2009). Therefore, given the critical role of both photosynthesis and g_s in determining land-atmosphere exchanges, their accurate representation and parameterisation in LSMs is of paramount importance. Booth et al. (2012) show that a significant uncertainty is the temperature sensitivity of photosynthesis, and suggest that thermal acclimation of photosynthesis – where plants adjust their optimum temperature for photosynthesis to growth conditions experienced over the timescale of days to weeks - might reduce the spread in modelled carbon exchange. Yet despite strong evidence of the thermal acclimation capability of plant photosynthesis (Dusenge et al., 2020; Slot et al., 2021; Way et al., 2017; Way and Yamori, 2014; Yamaguchi et al., 2016), incorporation of this process in large-scale LSMs is limited to only a few e.g. TEM (Chen and Zhuang, 2013), CLM4.5 (Lombardozzi et al., 2015), LM3 (Smith et al., 2016), JULES (Mercado et al., 2018), ORCHIDEE (Krinner et al., 2005) and BETHY (Ziehn et al., 2011), and is not yet commonly represented in ESMs. Currently, the majority of LSMs and ESMs use simple fixed (i.e. non-acclimating) temperature response functions for photosynthetic capacity parameters (Smith and Dukes, 2013), which, in general, cause the rate of leaf photosynthesis to increase with temperature to an optimum and then decrease under higher temperatures. These functional forms are either generic for all C_3/C_4 species and fixed in time and space, or are dependent on a small number of plant functional types (PFTs) but again fixed in time and space. Consequently, climate-carbon feedbacks in ESMs are sensitive to the assumed value of the fixed optimum temperature for photosynthetic capacity (T_{opt}), because, very simplistically, the amount of

104 carbon assimilated depends on whether leaf temperature is dominantly above or below T_{opt}. Improved process

105 representation of g_s, photosynthesis, and its temperature sensitivity in LSMs is necessary to support robust

106 predictions of global climate change via their coupling into ESMs. Modelling studies have shown how

107 photosynthesis and g_s impact climate feedbacks, play a critical role in how climate will change, and strongly

108 influence climate-induced impacts such as water resources (Betts et al., 2007; Cruz et al., 2010; De Arellano et

109 al., 2012; Gedney et al., 2006; Kooperman et al., 2018; Zeng et al., 2017).

110 This study, therefore, updates the plant physiology routines in the Joint UK Land Surface Environment Simulator

111 (JULES-vn5.6) LSM, the land-surface component of the UK Hadley Centre ESM (Sellar et al., 2019). To date,

112 JULES has employed the mechanistic C_3 photosynthesis scheme of Collatz et al. (1991) ("Collatz"). However,

113 the Farquhar et al. (1980) ("Farquhar") scheme is more generally adopted by those modelling photosynthetic

114 response and by researchers analysing data from empirical studies. The Farquhar scheme has been recently

115 implemented in JULES by Mercado et al. (2018) for C_3 plant types, albeit using a big leaf canopy scaling approach

116 and was not parameterised and evaluated for global applications. Here we build on that previous study by using a

117 data-driven approach incorporating data from multiple biomes to parameterise the Farquhar model photosynthetic

118 capacity parameters and their temperature sensitivity so it is amenable for use in global studies. Our specific

119 rationale for including the Farquhar photosynthesis scheme is twofold. Firstly, studies by Rogers et al. (2017) and

120 Walker et al. (2021) demonstrate that despite only the Collatz or Farquhar descriptions of leaf photosynthesis

121 being in general use, simulated photosynthesis varies significantly between LSMs. This variation is attributed to

122 several factors, including 1) differences in prescribed Rubisco kinetic constants and their temperature responses

123 (Rogers et al., 2017), 2) structural differences, namely the method used to determine the transition point between

124 the limiting rates of photosynthesis which has a disproportionate impact on estimates (Huntingford and Oliver,

125 2021; Walker et al., 2021) , and 3) the sensitivity of photosynthesis to temperature, in terms of the under-

126 representation of parameters from different biomes to describe the short-term instantaneous response of

127 photosynthesis to temperature (Rogers et al., 2017). In particular, these differences imply that parameter values

128 derived calibrating the Collatz model against data will differ to those derived using Farquhar against the same set

129 of measurements. Parameter values are not transferable between models, hence such differences will lead to

130 inconsistencies and projection errors if parameters are fitted to data, but then applied within the alternative model.

131 Building in the capacity of an LSM to run with either photosynthesis scheme greatly enhances flexibility in

132 modelling. Importantly, this flexibility allows for consistency between parameters used by empiricists to derive

133 leaf level photosynthetic parameters from observations, and those used in large scale modelling. Additionally, our

134 re-parameterisation of the photosynthetic capacity and temperature sensitivity parameters are based on recent

135 global datasets that are more extensive, including species from a range of different biomes, further enhancing the

136 capacity for global modelling applications. Our second rationale is that the Farquhar photosynthesis scheme is

137 required as the underlying model to implement the Kattge and Knorr (2007) thermal acclimation scheme.

138 Leaf level g_s response to water vapour is commonly represented in LSMs empirically (Jarvis et al., 1976), or with

139 a semi-empirical model (Ball et al., 1987; Damour et al., 2010; Leuning, 1995). Values of g_s are subsequently

140 scaled yielding an estimate of canopy conductance for vegetation in different ecosystems. De Kauwe et al. (2013)

141 showed that 10 of the 11 ecosystem models studied in their inter-comparison used a form of the "Ball–Berry–

142 Leuning" approximation. This model form links g_s to changes in environmental conditions, and directly to

143   photosynthetic rate. However, there is increasing interest in using models based on optimisation theory (Franks et

144   al., 2017; Franks et al., 2018), using evidence that stomata may behave to maximise CO_2 gain whilst minimising

145   water loss. The major advantage of optimality theory is that the optimisation criterion will apply under any

146   environmental conditions, past or future. Hence the derived equations can replace uncertain mechanistic

147   formulations and may also have more predictive capability corresponding to future climate regimes. JULES

148   traditionally uses the empirically-based Jacobs (1994) g_s scheme ("Jacobs"), and in this study we compare the

149   behaviour of this scheme against the Medlyn et al. (2011) g_s scheme ("Medlyn") which is based on optimisation

150   theory. The Medlyn g_s model has been previously implemented in JULES by Oliver et al. (2018). However, in

151   this study, we advance on that previous work by calibrating for the increased number of plant functional types

152   now in JULES (nine PFTs, as opposed to five in the original study), and we parameterise using data from a global

153   synthesis of experimental observations.

154   There is increasing evidence that the short-term vegetation temperature responses are themselves sensitive to

155   temperatures experienced over longer time-scales (days to weeks to seasons) and in particular, have the capability

156   to acclimate to growth temperature (T_{growth}) (Kattge and Knorr, 2007). Observational evidence of thermal

157   acclimation of photosynthesis has been widely reported, primarily for temperate and boreal ecosystems (Atkin et

158   al., 2006; Gunderson et al., 2000; Gunderson et al., 2010; Hikosaka et al., 2007; Way and Yamori, 2014; Yamori

159   et al., 2014). The effect is defined as the fast temporal adjustment of the temperature response of photosynthesis

160   driven by a change in T_{growth}. Thermal acclimation of photosynthesis typically results in a shift in the optimum

161   temperature (T_{opt}) for photosynthesis towards the new growth temperature, which can result in an increase or

162   maintenance of the photosynthetic rate respective to T_{growth} (Yamori et al., 2014). In this study, we implement

163   thermal acclimation of photosynthetic capacity in JULES using the scheme from Kattge and Knorr (2007). The

164   scheme attributes all changes in the photosynthetic response to changing T_{growth}, without specifically separating

165   adaptation from acclimation processes. Of those LSMs that do account for thermal acclimation of photosynthesis

166   (e.g. TEM, CLM4.5, LM3, JULES) (Chen and Zhuang, 2013; Lombardozzi et al., 2015; Mercado et al., 2018;

167   Smith et al., 2016), all similarly use this numerical algorithm from Kattge and Knorr (2007). Mercado *et al* (2018)

168   investigated the impacts of thermal acclimation on the future land carbon sink using an implementation of the

169   Kattge and Knorr (2007) in JULES, although using a simple big leaf scaling approach. In this study we apply the

170   thermal acclimation scheme in the updated JULES model (i.e. newly parameterised Farquhar scheme, running

171   with a multi-layer canopy and nine PFTs) and updated with the Medlyn g_s scheme and related parameters.

172   This paper therefore brings together these three key recent developments of the JULES plant physiology routines,

173   (1) implementation of the Farquhar photosynthesis scheme, (2) the optimisation-based Medlyn model of stomatal

174   opening, and (3) thermal acclimation of photosynthesis, along with updated parameters and an evaluation of model

175   behaviour. We make incremental additions of the different processes to the JULES model in a set of factorial

176   simulations and run the model with current day (1979 to 2013) near-surface meteorological forcing and CO_2

177   levels. First, we present the different factorial simulations in the context of a thorough evaluation of simulated

178   contemporary carbon and energy fluxes. Such evaluation includes comparison against individual eddy covariance

179   sites, and at spatial scales up to the global scale against satellite products. Timescales analysed are both seasonal

180   and annual. Secondly, we apply the new model configurations within a past-to-future climate change simulation

181   based on a high-end emissions scenario (SSP5 RCP8.5). We use output from HadGEM3-GC.1 spanning years

182 1960 to 2050 to explore sensitivity of global vegetation to future climate change. This choice of scenario is to

183 allow eventual comparison between these offline simulations and the equivalent in the coupled global climate

184 model to investigate land-atmosphere feedbacks resulting from these changes to the plant physiology routines.

185 This is currently work being undertaken. This updated version of the JULES model is now available in official

186 JULES releases for use by the community (see data availability). It is therefore also readily available for full

187 coupling into the UK community ESM (UKESM), a process that is just starting.

188

189

190 **2. Model description**

191 **2.1 JULES land surface model**

192 Our modelling framework is JULES (https://jules.jchmr.org), the land surface component of the Hadley Centre

193 climate models, which includes the new UK community Earth System Model (UKESM1) (Sellar et al., 2019).

194 JULES can be run offline, as in this study, forced with observed meteorology, at different spatial scales (from a

195 single location to global). A full description of JULES is provided in Best et al. (2011), Clark et al. (2011) and

196 Harper et al. (2016). Of particular relevance for this study is the plant physiological representation in JULES.

197 JULES uses a leaf-level coupled model of photosynthesis and g_s (Cox et al., 1998) based on Collatz et al. (1991)

198 and Collatz et al. (1992) (for C_3 and C_4 plants) and Jacobs (1994) respectively. Photosynthesis and g_s are modelled

199 to respond to changes in environmental drivers of temperature, humidity deficit, light, CO_2 concentration and

200 water availability. Soil moisture content is modelled using a dimensionless soil water stress factor which is related

201 to the mean soil water concentration in the root zone, and the soil water contents at the critical and wilting point

202 (Best et al., 2011). In this study, JULES uses a multilayer canopy radiation interception and photosynthesis scheme

203 (i.e. 10 layers) that accounts for vertical variation of incoming direct and diffuse radiation, sun fleck penetration

204 through the canopy, change in photosynthetic capacity with depth into the canopy, inhibition of leaf respiration

205 in the light and differentiates calculation of sunlit and shaded photosynthesis at each layer (Clark et al., 2011;

206 Mercado et al., 2009).

207 **2.2 Physiology Developments**

208 **2.2.1 Farquhar photosynthesis for C_3 plants and parameterisation**

209 We implement the Farquhar photosynthesis scheme (Farquhar et al., 1980) to describe the leaf-level biochemistry

210 of photosynthesis for C_3 vegetation following the approach of Mercado et al. (2018). Here the leaf-level

211 photosynthesis is calculated as the minimum (note no smoothing) of two potentially limiting rates (Equation 1a).

212 These two rates are i) Rubisco-limited photosynthesis (Equation 2) and ii) light-limited photosynthesis with a

213 dependence on the incident photosynthetically active photon flux density and the potential electron transport rate

214 (Equations 3 and 4). Note, as in the original Farquhar formulation, we do not include a TPU-limited (triose

215 phosphate utilisation) rate. Further, recent empirical studies suggest that TPU limitation rarely limits

216 photosynthesis under present-day CO_2 concentrations and is also unlikely to limit photosynthesis at elevated CO_2

217 (Kumarathunge et al., 2019a). This, and the current uncertainty in the formulation of TPU limitation of

218 photosynthesis led Rogers et al. (2021) to conclude it is an unnecessary complication in LSMs. Hence:

$$A_p = min\{A_v, A_j\} - R_d \tag{1a}$$

$$A_n = A_p\beta \tag{1b}$$

where A_p is the net potential (i.e. unstressed) leaf photosynthetic carbon uptake (mol m^2 s^{-1}), R_d is the rate of leaf respiration in the dark (mol m^2 s^{-1}), A_n is the net photosynthetic rate (mol m^2 s^{-1}) which accounts for the impact of soil moisture stress on photosynthetic rate by multiplying A_p by the soil water stress factor β. Rubisco-limited photosynthesis (A_v, mol m^2 s^{-1}) is calculated as in Equation 2. The maximum rate of carboxylation of Rubisco is determined by V_{cmax} (mol m^2 s^{-1}), c_i and o_a are the intercellular concentrations of CO_2 and O_2 (both Pa), K_c and K_o (both units of Pa) are the Michaelis Menten coefficients for Rubisco carboxylation and oxygenation respectively, and Γ (Pa) is the CO_2 compensation point in the absence of mitochondrial respiration.

$$A_v = \frac{V_{cmax}\,(c_i - \Gamma)}{\left[c_i + K_c\left(1 + \frac{o_a}{K_o}\right)\right]} \tag{2}$$

The light-limited rate of photosynthesis (A_j, mol m^2 s^{-1}) (Equation 3) is a function of the rate of electron transport J (mol m^2 s^{-1}) which is represented in Equation 4. J depends on the incident photosynthetically active photon flux density Q (mol quanta m^2 s^{-1}), the potential rate of electron transport J_{max} (mol m^2 s^{-1}), and the apparent quantum yield of electron transport α (mol electrons mol^{-1} photon), fixed at 0.3 (mol electrons mol^{-1} photon) following Medlyn et al. (2002). The factor of four used in the Farquhar model in Equation 3 accounts for four electrons being required per carboxylation/oxygenation reaction.

$$A_j = \left(\frac{J}{4}\right)\frac{(c_i - \Gamma)}{(c_i + 2\Gamma)} \tag{3}$$

$$\theta J^2 - (\alpha Q + J_{max})J + \alpha Q J_{max} = 0 \tag{4}$$

JULES currently uses Q_{10} functions in the Collatz scheme to describe the temperature dependency of K_c, K_o, and Γ. In our implementation of the Farquhar scheme, temperature sensitivities for the latter parameters are taken from Bernacchi et al. (2001) as described in Medlyn et al. (2002). These are the same temperature sensitivities used by experimentalist to derive estimates of photosynthetic capacity parameters (Rogers et al., 2017). Of particular importance to our analysis here are the temperature responses of V_{cmax} and J_{max}. Equation 5 describes the temperature response of both parameters:

$$k_T = k_{25}\,exp\left[H_a\frac{(T_l - T_{ref})}{T_{ref}\,R\,T_l}\right]\frac{1 + exp\left[\frac{T_{ref}\,\Delta S - H_d}{T_{ref}\,R}\right]}{1 + exp\left[\frac{T_l\,\Delta S - H_d}{T_l\,R}\right]} \tag{5}$$

Here, k_T (µmol m^2 s^{-1}) is either V_{cmax} or J_{max} at leaf temperature T_l (K), k_{25} (µmol m^2 s^{-1}) is the rate of V_{cmax} or J_{max} at the reference temperature T_{ref} of 25 ℃ (298.15 K), R is the universal gas constant (8.314 J K^{-1}), H_a and H_d (J mol^{-1}) are the activation and deactivation energies respectively, and ΔS (J mol^{-1} K^{-1}) is an entropy term (see Table

251   1 for PFT-specific parameter values). Broadly, H_a describes the rate of exponential increase of the function below

252   the optimum temperature (T_{opt}), and H_d describes the rate of decrease above the T_{opt}. ΔS and T_{opt} are related by

253   Equation 6, which is used to calculate the T_{opt} of V_{cmax} and J_{max} (Table 1):

254

255   $$T_{opt} = \frac{H_d}{\Delta S - R \ln\left[\frac{H_a}{H_d - H_a}\right]}$$ (6)

256

257   **Table 1.** PFT-specific parameters for the required temperature dependency of V_{cmax} and J_{max} in the Collatz and

258   Farquhar photosynthesis schemes. PFT codes (left column) are BET-tr: Broadleaf evergreen tropical tree, BET-

259   te: Broadleaf evergreen temperate tree, BDT: Broadleaf deciduous tree, NET: Needle leaf evergreen tree, NDT:

260   Needle leaf deciduous tree, C_3: C_3 grass, C_4: C_4 grass, ESH: Evergreen shrub, DSH: Deciduous shrub.

261

	Collatz			Farquhar						
	T_{upp}	T_{low}	$Topt_{vcmax}$	Ha_{vcmax}	Ha_{jmax}	ΔS_{vcmax} (J mol^{-1} K^{-1})	ΔS_{jmax} (J mol^{-1} K^{-1})	$Topt_{vcmax}$	$Topt_{jmax}$	Hd_{vcmax} or Hd_{jmax}
	(°C)	(°C)	(°C)	(J mol^{-1})	(J mol^{-1})			(°C)	(°C)	(J mol^{-1})
BET-tr	43	13	39.00	86900	64000	631	635	42.71	38.73	200000
BET-te	43	13	39.00	59600	35900	634	632	38.80	37.10	200000
BDT	43	5	39.00	49300	38800	658	663	26.57	23.22	200000
NET	37	5	33.00	63100	36400	642	643	35.28	31.96	200000
NDT	36	-5	34.00	49300	38800	658	663	26.57	23.22	200000
C_3	32	10	28.00	97200	112000	660	663	28.00	28.00	199000
C_4	45	13	41.00	-	-	-	-	-	-	-
ESH	36	10	32.00	59600	35900	634	632	38.80	37.10	200000
DSH	36	0	32.00	49300	38800	658	663	26.57	23.22	200000

262

263

264

265   To find new estimates for V_{cmax} and the J_{max}:V_{cmax} ratio at T_{ref} of 25°C for use with the Farquhar model for the 9

266   PFT's in JULES we used the global dataset from Walker et al. (2014) which includes data from 356 species. For

267   V_{cmax} and J_{max}, Walker et al. (2014) re-analysed the data to remove the variation in these two parameters across

268   studies caused by different parametric assumptions used in their derivation from A-C_i curves (e.g. using a common

269   set of kinetic parameters, and reporting values at 25°C). We calculated the mean V_{cmax} and J_{max} across studies

270   conducted at ambient CO_2 concentration for each of the JULES PFTs (Table 2). To parameterise the deciduous

271   needleleaf tree (NDT) PFT, we use the values for the evergreen needleleaf tree (NET) PFT because the data for

272   NDT was from a single study on one juvenile (3 years old) species. An exception was the tropical broadleaf

273   evergreen tree (BET-tr) PFT, where we use V_{cmax} and J_{max} from the dataset collated in the more recent compilation

274 by Kumarathunge et al. (2019b), as this study includes many more tropical tree species than any previous meta-
275 analysis.

276 Parameter values for the temperature response functions for V_{cmax} and J_{max} (Equation 5) in the Farquhar scheme
277 were taken from a global dataset of photosynthetic CO_2 response curves, which entrained data from 141 C_3
278 species, ranging from the tropical rainforest to Arctic tundra (Kumarathunge et al., 2019b). The study provides
279 parameter values for tree PFT's that match those in JULES, e.g. tropical broadleaf evergreen trees (BET-tr PFT
280 in JULES), temperate broadleaf evergreen trees (BET-te), broadleaf deciduous trees (BDT) and needleleaf
281 evergreen trees (NET). For the remaining JULES PFTs, BDT values are used for NDT and deciduous shrubs
282 (DSH), and BET-te values are used for evergreen shrubs (ESH). Kumarathunge et al. (2019b) do not include data
283 for C_3 grasses, therefore to parameterise the temperature dependency of V_{cmax} and J_{max} for this PFT, we fitted both
284 to the existing V_{cmax} temperature response function in the Collatz scheme for C_3 grasses because of a scarcity of
285 data in the literature. Fig. S1 shows the temperature dependency of V_{cmax}, J_{max} and gross photosynthesis for Collatz
286 and Farquhar using the PFT-specific parameters in Table 1 and Table 2.

287

288 **Table 2.** PFT-specific parameters for the Collatz and Farquhar photosynthesis schemes.

289

	Collatz		Farquhar			
	V_{cmax25} (umol m^{2}s^{-1})	α _(intrinsic)_ (mol CO$_2$ mol^{-1} PAR)	V_{cmax25} (umol m^{2}s^{-1})	J_{max25} (umol m^{2}s^{-1})	J:V	α _(apparent)_ (mol electrons mol^{-1} photon)
BET-tr	41.16	0.08	39.50	63.20	1.60	0.30
BET-te	61.28	0.06	68.95	112.59	1.63	0.30
BDT	57.25	0.08	55.24	98.30	1.78	0.30
NET	53.55	0.08	50.80	75.14	1.48	0.30
NDT	50.83	0.10	50.80	75.14	1.48	0.30
C_3	51.09	0.06	43.83	108.07	2.47	0.30
C_4	31.71	0.04	-	-	-	-
ESH	62.41	0.06	68.96	112.59	1.63	0.30
DSH	50.40	0.08	55.24	98.30	1.78	0.30

290

291

292 **2.2.2 Medlyn model of g_s and parameterisation**

293 In JULES, g_s (m s^{-1}) is represented in Equation 7.

294 $$g_s = 1.6RT_l \frac{A_n}{c_a - c_i}$$ (7)

295 where the factor 1.6 accounts for g_s being the conductance for water vapour rather than CO_2, R is the universal
296 gas constant (J K^{-1} mol^{-1}), T_l is the leaf surface temperature (K), c_a and c_i (both Pa) are the leaf surface and internal
297 CO_2 partial pressures respectively, and A_n is the net photosynthetic rate. Here, c_i is unknown and is calculated in

298   JULES using the Jacobs scheme as in Equation 8, and relates the ratio of ambient (c_a) to leaf intercellular (c_i)

299   partial pressure of CO_2 (c_i/c_a), to leaf humidity deficit:

300    $$c_i = (c_a - \Gamma)f_0 \left(1 - \frac{d_q}{d_{q_{crit}}}\right) + \Gamma \qquad (8)$$

301   where Γ (Pa) is the CO_2 photorespiration compensation point, d_q is the humidity deficit at the leaf surface (kg kg⁻

302   ¹), and $d_{q_{crit}}$ (kg kg⁻¹) and f_0 are PFT specific parameters representing the critical humidity deficit at the leaf surface

303   and the leaf internal to atmospheric CO_2 ratio (c_i/c_a) at the leaf specific humidity deficit (Best et al., 2011). To

304   implement the Medlyn model, Equation 9 is used to calculate c_i, retaining Equation 7 to calculate g_s. In Equation

305   9, g_1 ($kPa^{0.5}$) is a PFT-specific model parameter and d_q is expressed in kPa. The Medlyn scheme is based on

306   optimisation theory, and so assumes that stomatal aperture is regulated to maximize carbon gain while

307   simultaneously minimising water loss:

308    $$c_i = c_a \left(\frac{g_1}{g_1 + \sqrt{d_q}}\right) \qquad (9)$$

309   PFT-specific values of the g_1 parameter were derived for the nine JULES PFTs from the global data base of Lin

310   et al. (2015) (Table 3). The g_1 parameter represents the sensitivity of g_s to the assimilation rate, i.e. plant water

311   use efficiency, and was derived as in Lin et al. (2015), by fitting the Medlyn et al. (2011) model to observations

312   of g_s, photosynthesis, and VPD, assuming an intercept of zero.

313

314   **Table 3.** PFT-specific parameters required for the Jacobs and Medlyn g_s schemes.

315

	Jacobs f_o	Jacobs $d_{q_{crit}}$ (kg kg⁻¹)	Medlyn g_1 ($kPa^{0.5}$)
BET-tr	0.875	0.090	5.31
BET-te	0.892	0.090	3.37
BDT	0.875	0.090	4.45
NET	0.875	0.060	2.35
NDT	0.936	0.041	2.35
C₃	0.931	0.051	5.25
C₄	0.800	0.075	1.62
ESH	0.950	0.037	3.29
DSH	0.950	0.030	5.47

316

317   **2.2.3 Thermal acclimation of photosynthetic capacity**

318   The Kattge and Knorr (2007) acclimation algorithm ("AcKK") is based on the parameters of the Farquhar

319   photosynthesis scheme, hence acclimation is implemented in the Farquhar model. The AcKK algorithm uses

320   empirical relationships to describe the response of V_{cmax}, J_{max}, and the $J_{max}:V_{cmax}$ ratio to changes in T_{growth} (defined

321   in AcKK as the average temperature (day and night) of the previous 30 days), and importantly it represents

322 combined acclimation and adaptation processes. Kattge and Knorr (2007) found that ΔS_v, ΔS_j, and the J_{max}:V_{cmax}

323 ratio decrease linearly with increasing T_{growth} following Equation 10. This means according to these relationships,

324 the optimum temperatures (T_{opt}) of V_{cmax} and J_{max} (T_{optv} and T_{optj}) increase by 0.44°C and 0.33°C per degree increase

325 in T_{growth} respectively, and the J_{max}:V_{cmax} ratio at 25°C decreases by 0.035°C per degree increase in T_{growth}.

326 $$x_i = a_i + b_i\, T_{growth} \tag{10}$$

327 The x is either ΔS_v, ΔS_j or the J_{max}:V_{cmax} ratio, and the sub-index i refers to the parameter values (a and b shown in

328 Table 4) for V_{cmax}, J_{max} or the J_{max}:V_{cmax} ratio. T_{growth} is the growth temperature (calculated online as the mean

329 temperature of the previous 30 days).

330

331 **Table 4.** Parameter values derived by Kattge & Knorr (2007) and used in this study in Equation 10 to model

332 thermal acclimation of photosynthesis using the AcKK scheme.

	Acclimation	
	a	b
ΔS_j	659.7	-0.75
ΔS_v	668.39	-1.07
J_{max}:V_{cmax}	2.59	-0.035

333

334

335 **3. Model evaluation and application**

336 **3.1 Site level simulations**

337 JULES was applied using four model configurations (Table 5) with observed meteorology, and evaluated against

338 data from 17 eddy covariance sites (Table S1). This collection of eddy covariance measurements represents a

339 range of climates and land cover types (Table S1). In all simulations the vegetation cover was prescribed,

340 removing any biases that the modelled competition may introduce through self-diagnosis of PFT extents.

341 Prescribed leaf area index (LAI) was used where site data was available, otherwise the JULES phenology scheme

342 was switched on allowing the model to evolve the LAI. Model output was evaluated against fluxes of gross primary

343 productivity (GPP) and evaporative fraction (EF). We used EF rather than latent heat flux to minimise issues with

344 incomplete closure of the energy balance (that can typically range from 5 to 30 % at some eddy covariance sites,

345 Liu et al. (2006)). For analysis we used daytime values only (i.e. where the shortwave radiation was > 10 W m^2)

346 from days with no missing data, and compare mean seasonal diurnal cycles of modelled GPP and EF against the

347 observed fluxes.

348 We evaluate the site-level simulations with RMSE (root mean square error) using the relative improvement for
349 each model configuration (i) compared to the current standard JULES configuration of Collatz with Jacobs
350 (Clz.Jac). The statistic is calculated so that positive values show an improvement:

351 $$RMSE_{rel_i} = \frac{RMSE_{Clz.Jac} - RMSE_i}{RMSE_{Clz.Jac}} \qquad\qquad (11)$$

352

353 **Table 5.** Description of the four model experiments performed both at site level and globally, with the JULES
354 land surface model.

355

Model simulation	Description	Photosynthesis scheme	Stomatal closure	Temperature dependency of photosynthesis	T_{growth}
Clz.Jac	The original photosynthesis and stomatal conductance (g_s) schemes used in JULES.	Collatz *et al.*, (1991)	Jacobs (1994)	Q_{10} function for K_c, K_o Γ and V_{cmax} (PFT specific). T_{opt} varies by PFT but is fixed spatially and temporally.	NA
Fq.Jac	The Farquhar photosynthesis scheme is implemented with updated V_{cmax} and J_{max} values, and updated parameters for the temperature response of photosynthesis (ΔS and H_a for V_{cmax} and J_{max}) with original g_s scheme used in JULES.	Farquhar *et al.*, (1980)	Jacobs (1994)	Arrhenius function for K_c, K_o Γ, V_{cmax} and J_{max} (latter two both PFT specific). T_{opt} varies by PFT but is fixed spatially and temporally.	NA
Fq.Med	The Medlyn stomatal closure is implemented with the parameter g_1 that varies by PFT with Farquhar photosynthesis model implementation.	Farquhar *et al.*, (1980)	Medlyn *et al.*, (2011)	Arrhenius function for K_c, K_o Γ, V_{cmax} and J_{max} (latter two both PFT specific). T_{opt} varies by PFT but is fixed spatially and temporally.	NA
AcKK.Med	Thermal acclimation of photosynthetic capacity accounted for. Implemented within the Farquhar model coupled to the Medlyn g_s model.	Farquhar *et al.*, (1980)	Medlyn *et al.*, (2011)	Arrhenius function for K_c, K_o Γ. Thermal acclimation of photosynthetic capacity implemented following Kattge & Knorr (2007). Parameters describing the temperature sensitivity of photosynthesis (ΔS for V_{cmax} and J_{max}, and the J_{max}:V_{cmax}) allowed to acclimate to the temperature of the growth environment (T_{growth}). T_{opt} adjusts to changes in T_{growth} so varies spatially and temporally.	Yes

356

3.2 Global scale simulations

Four JULES simulations were performed globally for the period 1979-2013 as outlined in Table 5. These global present-day simulations were run at 0.5° x 0.5° spatial resolution. The WFDEI meteorological dataset was used to drive the model (Weedon et al., 2014). This has a three hour temporal resolution that JULES interpolated down to an hourly model time step. To focus on the direct effects of the model changes on GPP and surface energy fluxes, the land surface properties of the model were prescribed. We use a static map of land cover (in terms of different PFT extents) derived from the European Space Agency's Land Cover Climate Change Initiative (ESA LC_CCI) global vegetation distribution version 1.6 for the 2010 epoch (Poulter et al., 2015) (Fig. S3) following that used in Harper et al. (2016). Seasonally varying *LAI*, were derived from the Global LAnd Surface Satellite (GLASS) dataset (Xiao et al., 2016). We also prescribe transient atmospheric CO_2 concentrations based on annual mean observations from Mauna Loa (Tans and Keeling, 2014). A spin-up of 80 years was performed (re-cycling through the period 1979 to 1999), which is sufficient to equilibrate soil temperature and soil moisture.

The global offline present-day simulations were compared against the global evaluation products, and for both model output and observations we calculate seasonal means over the period 2002 to 2012. We used the global FluxCom product to evaluate modelled GPP, LE, H and ET (Jung et al., 2020; Tramontana et al., 2016). We compare our simulations against the FluxCom ensemble product (RS+MET) driven with the same forcing (WFDEI), as is recommended by Jung et al. (2019) to minimise deviations due to different climate input data. To convert LE to ET we assume a constant latent heat of vaporization of 2.5 MJ mm^{-1}. We also use the model derived product from GLEAM-v3.3a to evaluate ET, and additionally use the MODIS GPP product (Zhao et al., 2005; Zhao and Running, 2010; Zhao et al., 2006) to evaluate simulated global GPP**.**

Global future climate simulations were performed forced with meteorological output (1960 to 2050) from the HadGEM3-GC3.1 model atmosphere-only simulations at 3 hour temporal resolution and N512 spatial resolution (Roberts et al., 2019; Williams et al., 2018). These projections follow the CMIP6 HighResMIP protocol (Haarsma et al., 2016). This choice of forcing to drive JULES is to allow comparison of the offline runs performed in this study with the equivalent simulations currently being undertaken in the coupled HadGEM3-GC3.1 model to explore land-atmosphere feedbacks arising from changes implemented to the plant physiology routines in this work. The factorial set of offline simulations in this work provide a systematic sensitivity study that is less computationally expensive with which to help understand behaviour seen in the coupled model. The output at N512 was re-gridded to 0.5° x 0.5° using conservative interpolation. Fig. S4 shows the mean temperature and precipitation change by region over the study period, and the atmospheric CO_2 concentration. Atmospheric CO_2 concentrations were prescribed based on observations up to 2014 as described in historical CMIP6 simulations (Eyring et al., 2016). From 2015 onwards, atmospheric CO_2 concentrations were based on a high-end emission scenario of the Shared Socioeconomic Pathways (SSP5) with the Representative Concentration Pathway 8.5 (RCP8.5) (Haarsma et al., 2016). As for the current-day simulations, *LAI* and land cover were prescribed using the same datasets. A spin-up period of 80 years (re-cycling through the period 1960 to 1980) was again used to equilibrate soil temperature and soil moisture.

We analyse the future global simulations using the 'difference of difference' approach. This method explicitly targets the change in the variable of interest over the study period resulting from the change in process alone, and

395 negates differences that may arise from different initial starting points of each simulation (different initial

396 conditions):

397 $Effect = (\bar{X}_{2050} - \bar{X}_{1980}) - (\bar{Y}_{2050} - \bar{Y}_{1980})$ (12)

398 where X and Y represent the simulation with and without the process respectively, and 2050 and 1980 represent

399 the end and start of the simulation analysis period respectively (calculated as the mean over 2040 to 2050, and

400 1980 to 1990 respectively).

401

402 **4. Results**

403 **4.1 Site level evaluation**

404 Results from the FLUXNET sites comparing the mean seasonal diurnal cycles of GPP and EF against observed

405 fluxes are summarised in Fig. 1, where reds and yellows indicate reduced RMSE relative to the 'standard' JULES

406 configuration of Collatz with Jacobs (Clz.Jac), and therefore closer agreement to site level FLUXNET

407 observations. Results are variable by site and season, some of which will be due to other site-specific

408 characteristics that are not simulated well by the model, such as *LAI* for those sites that rely on model derived

409 estimates. On the other hand, soil properties are prescribed by parameters that describe the thermal and hydraulic

410 characteristics of the soil, uncertainties in these parameterisations have consequences for the simulated soil

411 moisture content at each site, for example, which impacts simulated carbon and water fluxes. We first consider

412 results for the five tropical sites. Results are mixed for the simulated seasonal diurnal cycle of GPP at the tropical

413 (EBF / BET-tr) sites, GPP is improved (reduced) with the new JULES model configurations at three out of the

414 five tropical sites in March-April-May (MAM; Fig. 1a), with thermal acclimation leading to the greatest

415 improvements. However in June-July-August (JJA; Fig. 1b), this improvement is only found at two of the tropical

416 sites. At the EBF sites, implementing the Farquhar photosynthesis model means V_{cmax} is lower (BET-tr, Table 2),

417 and this in addition to the change in temperature sensitivity (Table 1; Fig. S1a-c), and model structural changes

418 from Collatz to Farquhar results in lower simulated GPP compared to Collatz. Thermal acclimation allows further

419 adjustments of the $T_{opt}v$, $T_{opt}j$ and the $J_{max:}V_{cmax}$ ratio which results in lower simulated photosynthesis and therefore

420 GPP compared to Farquhar. The change from Jacobs g_s model to Medlyn has minimal impact on simulated GPP

421 for the tropical tree PFT because in both schemes the modelled c_i has a similar sensitivity to humidity deficit at

422 the leaf surface, with the exception at very low humidity deficit (Fig. S5). The simulated seasonal diurnal cycle

423 of EF is improved (reduced) at four out of the five tropical sites in both MAM and JJA, again with some of the

424 largest improvements seen with thermal acclimation (Fig. 1c & 1d).

425 At the C_3 grassland sites (GRA), improved simulated GPP (higher GPP) is seen across all sites in JJA with the

426 Medlyn g_s scheme and thermal acclimation (Fig. 1b). This is matched by improvements in simulated EF (higher

427 EF) across all grassland sites in both seasons, with the exception of US_var in JJA (Fig. 1c & 1d). The change

428 from Collatz to Farquhar at the GRA sites means a lower V_{cmax} is used (C3, Table 2) although the temperature

429 sensitivity is similar (Table 1, Fig. S1p, q), this results in lower GPP simulated by Farquhar compared to Collatz

430 which compares worse to the observations (GPP and EF, Fig. 1). In contrast to using Farquhar with the Jacobs g_s

431 scheme, using Farquhar with the Medlyn scheme improves simulated GPP and EF, both are increased because for

432   the C3 grass PFT as the humidity deficit at the leaf surface increases c_i simulated by Medlyn is less sensitive

433   compared to Jacobs (Fig. S5), leading to higher c_i, higher net canopy photosynthesis and GPP, and higher

434   transpiration and LE. These results suggests the Medlyn scheme has a large impact on simulated carbon and water

435   fluxes for the C3 grass PFT in the JULES model. In JJA, the adjustment of the temperature sensitivity of

436   photosynthesis to the T_{growth} by the thermal acclimation scheme tends to increase GPP compared to Farquhar with

437   no acclimation, and this compares better to the observations.

438   At the broadleaf deciduous tree sites (BDT) simulated GPP is improved with all JULES model configurations in

439   MAM (higher GPP) at three out of the four sites (Fig. 1a). However in JJA improvements are mainly seen with

440   thermal acclimation (lower GPP compared to Fq.Med, Fig. 1b). Medlyn g_s performs worse at all sites in JJA

441   suggesting either the model formulation or parameters are not suitable to correctly capture stomatal behaviour in

442   this season for this PFT (Fig. 1b). Compared to Collatz, the Farquhar model for the BDT PFT uses a lower V_{cmax}

443   (Table 2) and has a considerably lower $T_{opt}v_{cmax}$ (Table 1; Fig. S1h), which means that at leaf temperatures below

444   ~22ºC, photosynthesis is higher with the Farquhar model, and above this photosynthesis is lower than Collatz

445   (Fig. S1g). Consequently, warmer temperatures in JJA lead to lower GPP simulated by Farquhar compared to

446   Collatz, and cooler temperatures in MAM result in slightly higher GPP with Farquhar compared to Collatz. Using

447   the Medlyn model means simulated c_i is more sensitive to increasing leaf humidity deficit for the BDT PFT (Fig.

448   S5). Medlyn simulates a lower c_i as humidity deficit increases compared to Jacobs which leads to lower GPP and

449   LE, the magnitude of which depends on the local site humidity conditions. In JJA the Medlyn g_s model performs

450   worse at all sites for GPP (Fig. 1b), although improvements in simulated EF are seen in JJA, where both Medlyn

451   and thermal acclimation improve model performance at three out of four BDT sites (Fig. 1d).

452   At the evergreen needleleaf sites (NET) the most consistent improvements to simulated GPP are seen with the

453   Farquhar model, where simulated GPP in JJA is substantially improved (GPP reduced) at three out of four sites

454   (Fig. 1b), in this season both Medlyn and thermal acclimation generate larger improvements in the simulated GPP

455   (reducing GPP further), but this is just at two out of the four sites. In our implementation of the Farquhar model,

456   the NET PFT has a lower V_{cmax} compared to Collatz (Table 2), and a slightly higher $T_{opt}v_{cmax}$ (Table 1, Fig. S1k).

457   The resulting shape of the temperature response curve for photosynthesis (Fig. S1j) means that at leaf temperatures

458   below ~10ºC Farquhar photosynthesis is higher. However above 10 ºC Farquhar photosynthesis is lower compared

459   to Collatz, resulting in simulated GPP in MAM that tends to be higher with Farquhar than Collatz, and in JJA the

460   opposite occurs. In MAM and JJA the Medlyn g_s model simulates some large improvements in EF; c_i simulated

461   by Medlyn is more sensitive to increasing leaf humidity deficit compared to Jacobs (Fig. S5), which results in

462   lower transpiration and EF, and this compares better to the observations.

463

464

465

466

467

468   **Figure 1.** Relative changes in RMSE for each JULES model configuration compared to Collatz with Jacobs

469   (Clz.Jac) for hourly daytime a) GPP (March-April-May), b) GPP (June-July-August), c) EF (March-April-May)

470   and d) EF (June-July-August). Reds and yellows are where RMSE is lower compared to the Clz.Jac JULES

471   configuration, and therefore indicates an improvement with that model configuration compared to the Fluxnet

472   observations. EBF: Broadleaf evergreen tropical tree, GRA: C$_3$ grassland, BDT: Broadleaf deciduous tree, NET:

473   Needle leaf evergreen tree.

474
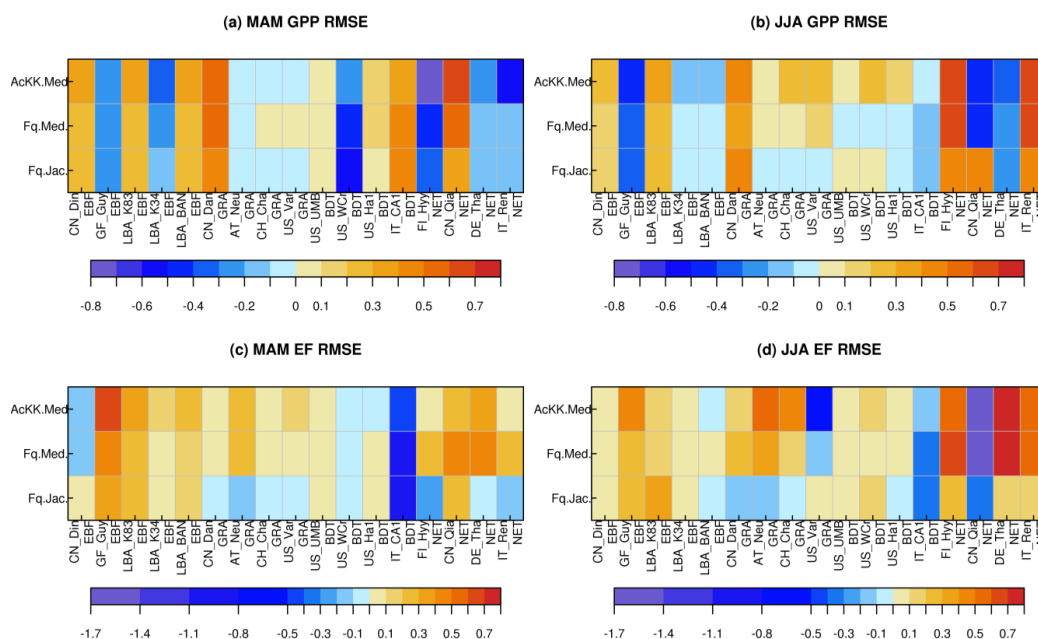
475

476

477

478

479   **4.2 Global Evaluation**

480   **4.2.1 Spatial differences between model configurations**

481   Figure 2 shows the JJA change in modelled GPP, LE and H with each of the new JULES configurations compared

482   to original JULES across the globe. For GPP, the biggest change is moving from the Collatz photosynthesis

483   scheme to the Farquhar photosynthesis scheme (Fig. 2a). Most notably, this change results in decreased GPP in

484   the tropical region in JJA of up to 1.5 gC m^{-2} d^{-1} (up to 10% reduction), whilst in the high northern latitudes, GPP

485   is increased by up to 1.5 gC m^{-2} d^{-1} (up to 20% increase). This is consistent with results from the site-level

486   simulations where GPP was reduced with implementation of the Farquhar model at tropical sites, and increased

487   in cooler months (MAM) at the evergreen needleleaf forest sites (here increased GPP in NET dominated areas are

488 in the forests of the high northern latitudes which is consistent with cooler temperatures). Impacts on LE and H

489 resulting from the move from Collatz to Farquhar are not as extensive as those seen with GPP (Fig. 2b & 2c). The

490 change from Jacobs g_s scheme to Medlyn impacts LE and H most, resulting in a pronounced pattern of decreased

491 LE in northern latitudes (up to 10 W m^{-2}, equivalent to a 10% reduction) and corresponding increase in H in JJA

492 (Fig. 2e & 2f). In these JULES simulations, this region is dominated by NET forest, and the high latitude changes

493 are consistent with results from the site-level simulations, where using the Medlyn g_s scheme at NET sites resulted

494 in some of the biggest improvements in simulated EF (lower LE and therefore lower EF). Including thermal

495 acclimation of photosynthesis has the most extensive impacts on simulated GPP in contrast to LE and H. In the

496 tropical forests GPP is reduced by up to 1 gC m^2 d^{-1} (between 2 to 5% reduction) in JJA (Fig. 2g). The impact of

497 acclimation is spatially variable in the temperate region in JJA, with GPP decreased in Europe (between 2 to 5%),

498 but increased in Eastern USA (up to 20%). Some areas of the boreal region see increased GPP (between 2 to 5%).

499 This GPP response demonstrates the impact of thermal acclimation which allows the parameters of the

500 temperature sensitivity functions for photosynthetic capacity (V_{cmax}, J_{max} and J_{max}:V_{cmax}) to move in response to the

501 temperature of the growth environment, leading to spatially and temporally different values of the T_{opt} for

502 photosynthesis for each C$_3$ PFT. Thermal acclimation impacts LE and H to a lesser extent, but where changes are

503 seen, acclimation increases LE with a corresponding decrease in H (Fig. 2h & 2i). Figs. 2j, 2k & 2l show the

504 overall change that results from moving from the traditional JULES set-up of Collatz with Jacobs (Clz.Jac) to

505 Farquhar with thermal acclimation and Medlyn g_s (AcKK.Med), and the impacts on simulated GPP, LE and H

506 can clearly be seen as the trade-off between the dominating effects from each model configuration. For LE and H

507 the response of the simulated energy fluxes is dominated by the change in the representation of g_s, and for GPP

508 the response of simulated carbon fluxes is dominated by the change in the representation of photosynthesis and

509 its response to temperature (i.e. thermal acclimation).

510

511

512

513

514

515

516

517

518

519

520

521

Figure 2. Differences between JULES modelled GPP, latent (LE) and sensible heat (H) for the different JULES

model configurations in June-July-August (JJA). For each variable the mean over the period 2002 to 2012 is used.

DJF is shown in Figure S6.
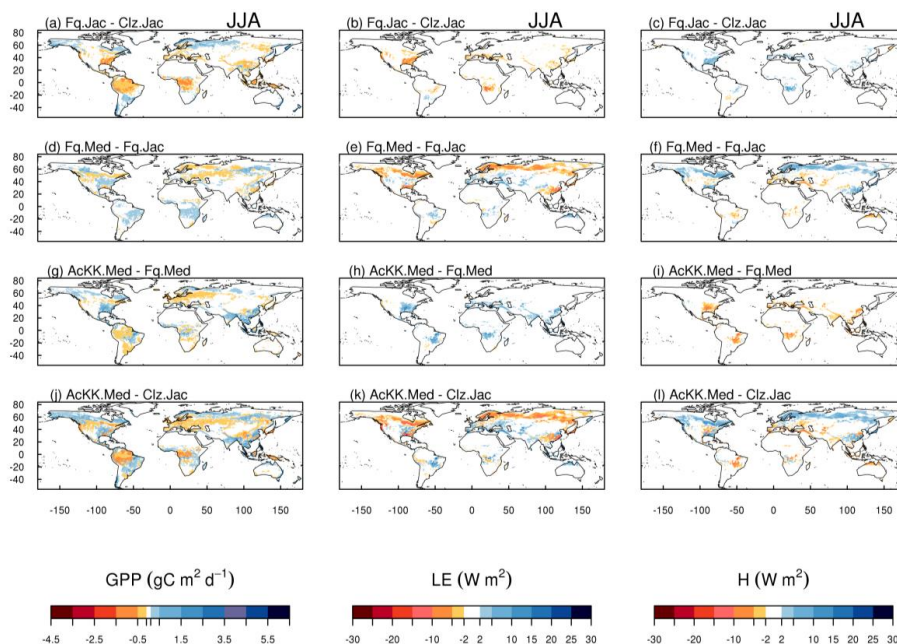
4.2.2 Comparison to global estimates: seasonal mean GPP and ET

Evaluation of simulated global mean GPP by season using FluxCom and MOD17 global GPP products is

presented in Fig. 3a and using global ET from both FluxCom and GLEAM is shown in Fig. 3b. The seasonal

means show thermal acclimation compares best to observations (FluxCom) in JJA (AcKK.Med underestimates

GPP by just 4%, whereas Clz.Jac underestimates GPP by 6%; Fig. 3a & Table S2) and MAM (AcKK.Med

underestimates GPP by just 5%, whereas Clz.Jac underestimates GPP by 11%; Fig. 3a & Table S2), and is in

reasonable agreement with FluxCom in DJF (AcKK.Med overestimates GPP by just 2%, whereas Clz.Jac

underestimates GPP by 4%; Fig. 3a & Table S2). All JULES model configurations have a high GPP bias in SON

compared to FluxCom, and in all seasons GPP is overestimated by all model configurations compared to MOD17,

similarly this is largest in SON. For simulated ET, seasonally the model performance is very similar between the

different JULES configurations, however in both SON and DJF Medlyn (Fq.Med) compares better to both

FluxCom and GLEAM, but the differences are very small (Fig. 3b & Table S3).

Figure 3. Seasonal mean global a) GPP and b) ET for each JULES model configuration compared to FluxCom (closed symbols) and MOD17 (GPP) or GLEAM (ET) (open symbols).
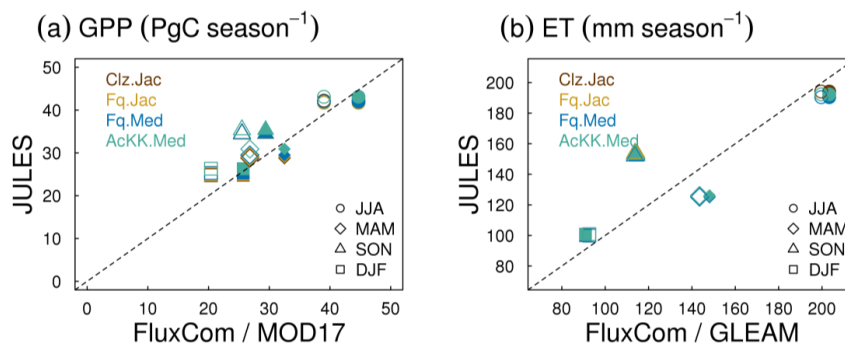
4.2.3 Comparison to global estimates: latitudinal mean GPP and ET

Figures 4 and 5 present comparisons of seasonal zonal-mean GPP and ET respectively. Firstly, Fig. 4 and Fig. 5 highlight the differences between global products used to evaluate GPP and ET (see e.g. Spafford & MacDougall 2021). For example, FluxCom generally predicts higher GPP in the tropics compared to MOD17, especially in DJF and MAM, and in JJA the different distribution of GPP by latitude means in the tropics MOD17 GPP is higher than FluxCom in the southern latitudes, and FluxCom GPP is higher in the northern tropics. Comparison of the two ET products shows that GLEAM tends to give higher ET in the tropics, particularly in DJF and MAM. Bearing in mind uncertainties in observation-based estimates of fluxes at this scale we now consider how the different model configurations compare. Notably, all the JULES model configurations in this study simulate comparable global carbon and water fluxes for the recent contemporary period and are in reasonable agreement with the global products used for evaluation. Differences in RMSE between the different model configurations are small for both GPP and ET. Importantly, the most consistent change is the improvement (lowest RMSE) of modelled GPP in the tropics with the Farquhar model (Fq.Jac). This improvement is evident in all seasons and holds when comparing to both FluxCom and MOD17 (Fig. 4). Similarly, estimates of ET are improved in the tropics (lowest RMSE) with the Farquhar model (Fq.Jac) in DJF and JJA, and with the Medlyn model (Fq.Med) in MAM and SON, and again this result is not dependent on the choice of observation-based product (Fig. 5). Another notable change is the improvement of simulated GPP in the temperate north and boreal regions in MAM with thermal acclimation (AcKK.Med). Deficiencies in the model stand out, but these biases are common to all model configurations. For example, all configurations simulate an over-prediction of GPP and ET in SON in the temperate north and boreal regions, overestimated GPP in MAM in tropical southern latitudes (0 to -20ºS), under-predicted GPP and ET in MAM in temperate north and boreal regions, and an over-prediction of ET in MAM in the temperate and tropical South.

Figure 4. Mean (2002 to 2012) GPP (g C m^2 d^{-1}) by latitude band and season for each JULES model configuration compared to the FluxCom and MOD17 global GPP products. The bars at the bottom indicate which model configuration gives the lowest RMSE, and therefore better comparison to FluxCom (top bar) and MOD17 (bottom bar) derived GPP for each region. RMSE values are shown in Tables S4 (FluxCom) and S5 (MOD17). The grey shaded area shows the uncertainty in the FluxCom GPP product, provided as the median absolute deviation of ensemble members, this is scaled to a robust estimate of the standard deviation of a normal distribution by multiplying by 1.4826 according to Jung *et al.*, (2019).
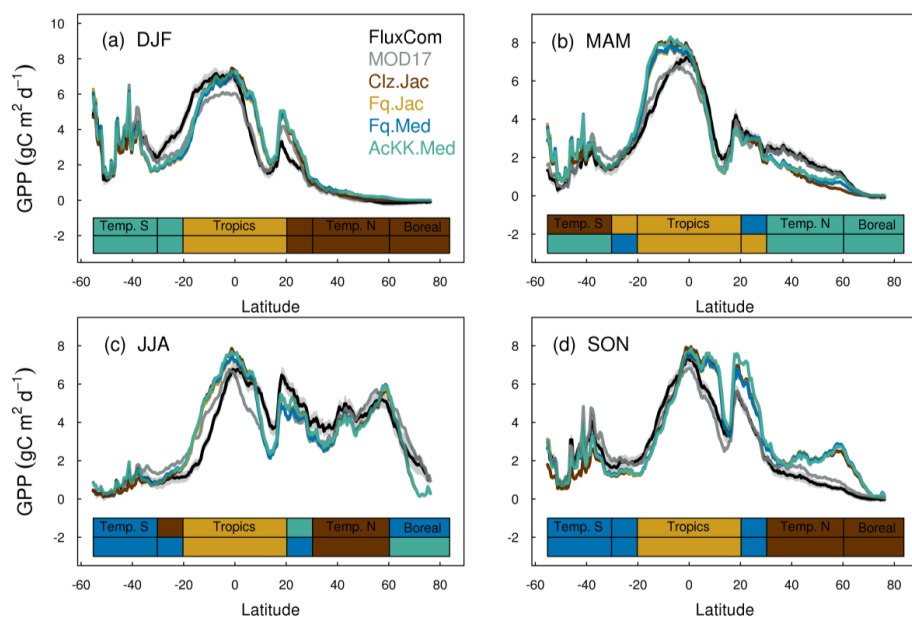
Figure 5. Mean (2002 to 2012) evapotranspiration (ET mm d^{-1}) by latitude band and season for each JULES model configuration compared to the FluxCom and GLEAM global ET products. The bars at the bottom indicate which model configuration gives the lowest RMSE, and therefore better comparison to FluxCom (top bar) and GLEAM (bottom bar) derived ET for each region. RMSE values are shown in Table S6 (FluxCom) and Table S7 (GLEAM). The grey shaded area shows the uncertainty in the FluxCom ET product, provided as the median absolute deviation of ensemble members, this is scaled to a robust estimate of the standard deviation of a normal distribution by multiplying by 1.4826 according to Jung *et al*., (2019).
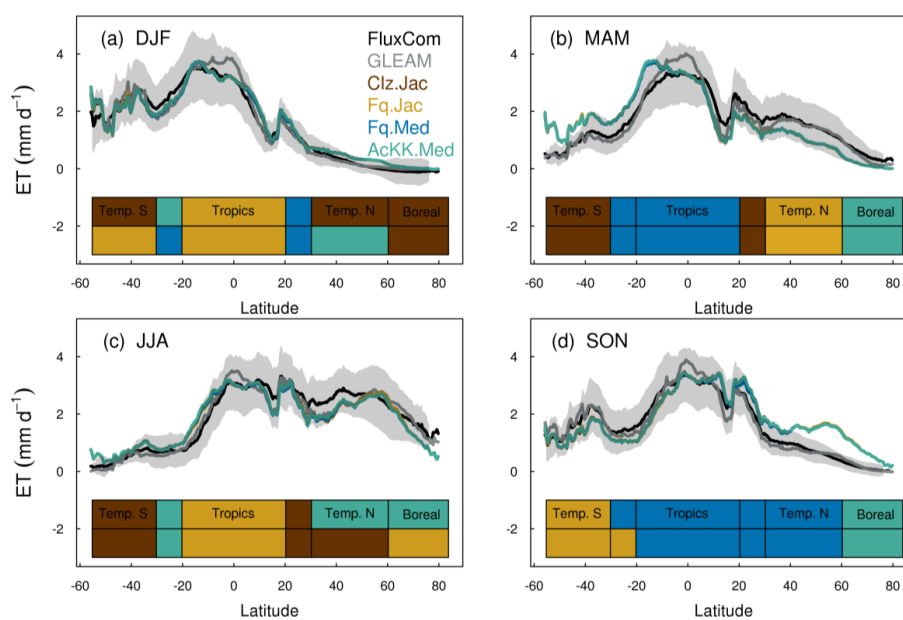
4.2.4 Comparison to global estimates: spatial variability of mean GPP and ET

The spatial variability of simulated GPP and ET is shown in Fig. 6 during JJA (Fig. S7 for DJF). We show which of the JULES model configurations gives the lowest RMSE compared to observation-based estimates of GPP and ET from FluxCom, MODIS and GLEAM (actual RMSE in Figs. S8 and S9). The differences in RMSE are typically small between the different JULES model configurations, however some clear patterns emerge. Figure 6a & b show that in the tropical forests (i.e. Amazon basin and central Africa) in JJA and DJF (Fig. S7a & b for DJF), GPP simulated including thermal acclimation (AcKK.Med) compares best to both FluxCom and MOD17. Also, in the high northern latitudes, dominated by evergreen needleleaf forests, inclusion of thermal acclimation more closely aligns simulated GPP with both FluxCom and MOD17 (Fig. 6a & b). Compared to FluxCom, ET in JJA is simulated best by thermal acclimation (AcKK.Med) in the northern temperate and boreal region, although this pattern is not consistent in comparison to GLEAM (Fig. 6c & d). In contrast to GPP, results are more mixed in the tropics for ET. In areas dominated by tropical tree cover, thermal acclimation (AcKK.Med) and Medlyn (Fq.Med) tend to give the lowest RMSE in JJA and DJF, and in tropical areas dominated by C_3 and C_4 grasses Farquhar (Fq.Jac) performs best (Fig. 6c & d), although in DJF the Medlyn model gives the lowest RMSE in these

609   areas (Fig. S7c & d). In DJF for both GPP and ET, in northern temperate and boreal regions the Collatz with

610   Jacobs (Clz.Jac) configuration performs the best (Fig. S7).

611

612   **Figure 6.** Colours indicate the JULES model configuration that gives the lowest RMSE compared to either the a)

613   FluxCom and b) MOD17 global GPP (gC m^2 day^{-1}) products, or c) FluxCom and d) GLEAM global ET (mm day^{-1}

614   ^{1}) products for JJA over the period 2002 to 2012. Actual RMSE values shown in Fig. S8 and Fig. S9.

615

616
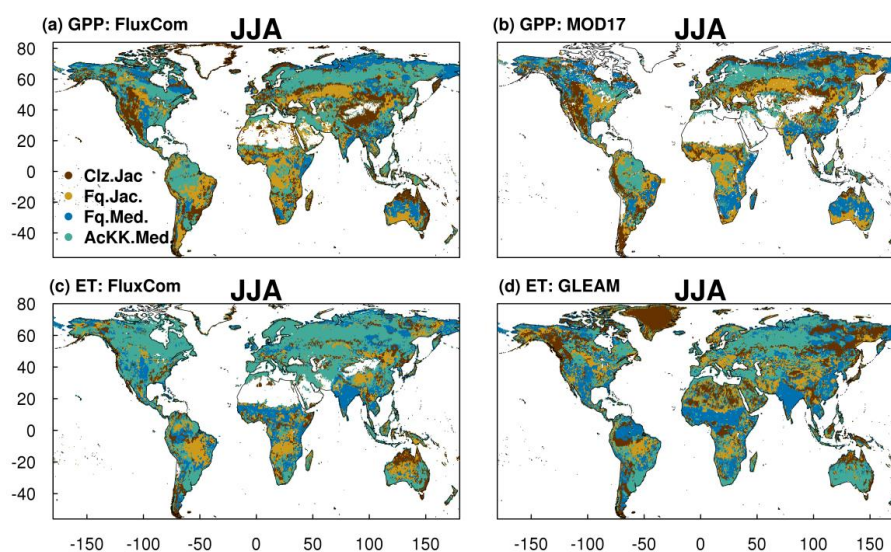
4.3 Application under future climate

618   We run the new configurations forced by variables from a future climate scenario (HadGEM3-GC3.1 forcing

619   under a high-end emission scenario of the SSPs) to investigate the response of simulated fluxes to long-term

620   warming. Changing the photosynthesis scheme from Collatz to Farquhar results in lower GPP, (up to 30%

621   decrease) by 2050 across the high northern latitude forests (Fig. 7a), with the impact on LE (decreased) and H

622   (increase) less extensive (Fig. 7b & c). This area is dominated by NET, NDT and BDT PFTs in JULES. The

623   different temperature sensitivity of photosynthesis parameterised with the Farquhar model compared to Collatz

624   (Fig. S1g, j & m) means at lower leaf temperatures, photosynthesis is higher with Farquhar, however, as leaf

625   temperature increases, photosynthesis falls in Farquhar relative to Collatz. The crossover point at which this

626   occurs is relatively low for these PFTs, particularly NET. This impact of the change of temperature sensitivity

627   was seen in the site-level simulations at FLUXNET NET and BDT sites. There, modelled GPP tended to be higher

628   with Farquhar than Collatz in MAM, but lower in the warmer conditions of JJA, and in this climate change

629   scenario the temperate and boreal region both experience large increases in mean annual air temperature (+5°C

630   from 1980 to 2060, Fig. S4a & c).

631 Replacing the Jacobs g_s scheme with Medlyn has the biggest impact on the surface energy fluxes, with increased

632 LE of up to 30% and a corresponding decrease in H by 2050 across the temperate region (Fig. 7e & f). This area

633 is dominated by the C3 grass PFT in JULES which has a less conservative water use strategy in the Medlyn

634 scheme (high g_1) compared to Jacobs. This means in the Medlyn scheme, the C3 grass PFT is less sensitive to

635 increasing humidity deficit at the leaf surface, therefore as humidity deficit increases Medlyn simulates higher c_i

636 leading to higher rate of transpiration and LE compared to Jacobs (Fig. S5).

637 Thermal acclimation of photosynthesis leads to widespread increases in GPP by 2050 (Fig. 7g). This amounts to

638 10% in the tropical forests, up to 30% in northern temperate and boreal regions, and up to 40% in south-east Asia.

639 In this long-term climate change scenario, with large increases in mean annual temperature (Fig. S4), the impact

640 of thermal acclimation on GPP can clearly be seen. The flexibility in $T_{opt}v$, $T_{opt}j$ and the $J_{max}{:}V_{cmax}$ ratio of

641 photosynthesis that thermal acclimation allows through letting these parameters move with the prevailing T_{growth},

642 allows for higher rates of photosynthesis and therefore GPP as temperatures increase. By contrast, in simulations

643 where photosynthetic rates are controlled by fixed temperature sensitivities, vegetation may have moved past its

644 thermal optimum. Time series of the area-weighted mean annual GPP show that in this simulation, across the

645 tropical region, thermal acclimation enhances GPP by ~7.5 PgC compared to no acclimation (Fig. 8a). In the

646 temperate region and sub-tropics thermal acclimation increases GPP by ~1 PgC by 2050 (Fig. 8b and d), and in

647 the boreal region GPP is enhanced by ~0.4 PgC (Fig. 8c). Thermal acclimation of photosynthesis also has a large

648 impact on simulated energy fluxes, most notably in the northern temperate region, where LE is increased by up

649 to 50 to 60% (decreased H up to 40 to 50%) (Fig. 7h & i).

650

651

652

653

654

655

656

657

658

659

660

661

662

Figure 7. The difference of difference approach (Equation 12) to determine the impact on GPP (g C m^2 day^{-1}), LE (W m^2) and H (W m^2) of the individual changes to each JULES model configuration over the course of the simulation (1980 to 2050) in June-July-August (JJA). For example, the AcKK.Med acclimation effect is calculated from Fig. S12 AcKK.Med – Fq.Med, the effect of the Medlyn g_s scheme is calculated from Fig. S12 Fq.Med – Fq.Jac, and the effect of the photosynthesis scheme is calculated from Fig. S12 Fq.Jac – Clz.Jac.
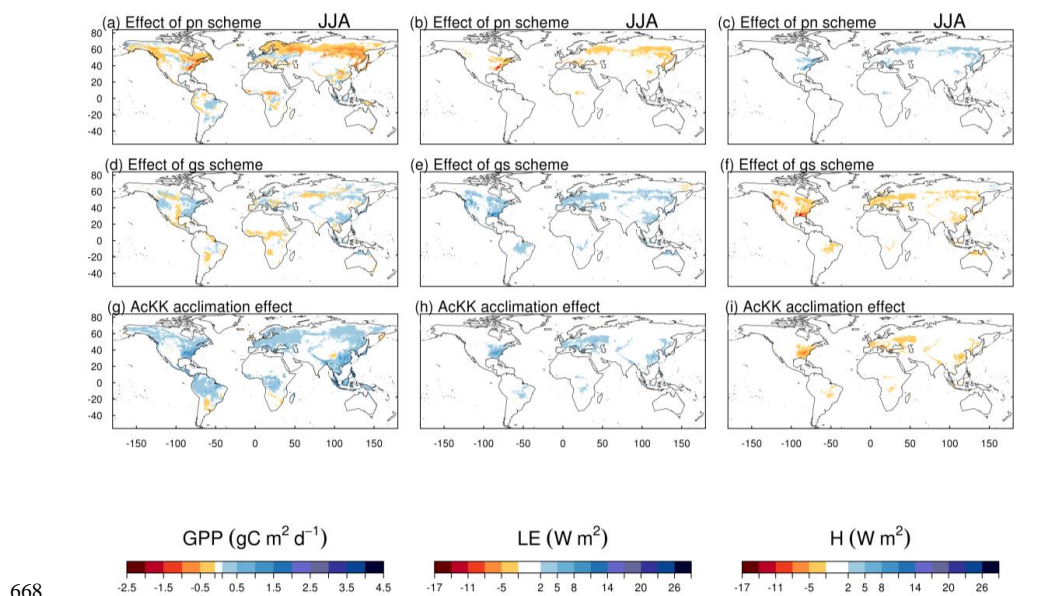
Figure 8. Time series of the regional mean acclimation effect i.e AcKK.Med – Fq.Med (black), and the effect of the Medlyn g_s model i.e. Fq.Med – Fq.Jac (grey).
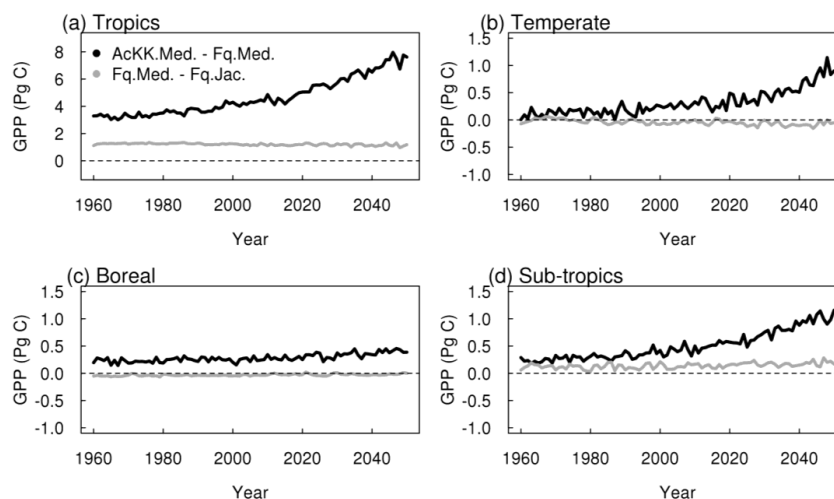
673 **5. Discussion**

674 Photosynthesis and g_s are central to the estimate of carbon and water fluxes in LSMs, and when coupled in ESMs

675 these processes feed-back onto the climate system to influence predictions of future climate change. Therefore

676 improving the representation of these processes in LSMs is important, and previous studies have identified thermal

677 acclimation of photosynthesis as a key missing process (Booth et al., 2012).

678

679 **5.1 Performance of the new JULES plant physiology model configurations: Thermal acclimation**

680 Our results show that including thermal acclimation of photosynthesis in the JULES model improves simulated

681 carbon and water fluxes in several key areas for the recent contemporary period. Firstly, the seasonal mean

682 estimates of global GPP show that in most seasons (JJA, MAM and DJF) thermal acclimation of photosynthesis

683 with Medlyn g_s (AcKK.Med) predicts GPP in closer agreement with estimates from FluxCom compared to the

684 traditional 'standard' JULES configuration of Collatz photosynthesis with Jacobs g_s (Clz.Jac). Secondly, thermal

685 acclimation with Medlyn g_s improves the simulation of GPP (reduces GPP) in the tropical forests in JJA and DJF

686 (i.e. the Amazon basin and central African rainforest region) and is in closest agreement with estimates of GPP

687 from both FluxCom and MOD17 for these regions. Thirdly, in the high northern latitude forests dominated by

688 evergreen needleleaved trees, thermal acclimation increases GPP in JJA and is again in closest agreement with

689 the observational estimates. Finally, in JJA, AcKK.Med improves the simulation of ET across a large area of the

690 temperate north and boreal regions.

691 Our evaluation therefore suggests that fixed, PFT-specific temperature dependencies for V_{cmax} (and J_{max}) do not

692 accurately simulate GPP for the tropical tree and evergreen needleleaf tree PFTs for the present-day in the JULES

693 model. Thermal acclimation allows the temperature sensitivity of photosynthesis to adjust to the local temperature

694 environment through flexibility in $T_{opt}v$, $T_{opt}j$ and the $J_{max}:V_{cmax}$ ratio. In the tropical forests, for example, GPP is

695 over-estimated by both Clz.Jac and Fq.Jac. The configuration with thermal acclimation reduces GPP compared to

696 both these model configurations. From the leaf-level plots in Fig. S1a, the fixed T_{opt} of photosynthesis in the

697 Collatz scheme is ~33ºC and in Farquhar is ~34ºC. This is higher than observations from Fig. 1a of Kumarathunge

698 et al. (2019b), where the T_{opt} for net leaf photosynthesis lies between ~29 to 32ºC, and other studies also show a

699 lower T_{opt} for photosynthesis of around 30ºC for mature tropical trees (Hernández et al., 2020; Mau et al., 2018).

700 This supports our results, and suggests the fixed temperature sensitivity of photosynthesis for tropical trees in the

701 JULES model results in a T_{opt} of photosynthesis that is too high for current-day. Thermal acclimation results in a

702 more realistic T_{opt} of photosynthesis for tropical trees because it is influenced by actual growth temperature and

703 so can adjust to local environmental conditions.

704 Under the climate change scenario used in this study, thermal acclimation shows a sustained positive acclimation

705 effect in all regions, increasing GPP in response to long-term warming (although this is less pronounced in the

706 boreal region). By 2050 GPP was ~10% higher with thermal acclimation in the tropical forests, up to 30 to 40%

707 higher across a large area of the northern hemisphere. Our findings broadly agree with Mercado et al. (2018), who

708 implemented the Kattge and Knorr (2007) thermal acclimation scheme into JULES running as part of a coupled

709 climate-carbon model, and found that thermal acclimation increased land carbon storage in tropical and temperate

710 regions. This is in contrast to Lombardozzi et al. (2015) and Smith et al. (2016) whose studies both found a

711 negative impact of photosynthetic thermal acclimation in the tropics, again using the Kattge and Knorr

712 (2007)thermal acclimation scheme. Mercado et al. (2018) attribute these differences to the method used to

713 implement acclimation of the $J_{max}:V_{cmax}$ ratio at 25ºC, that is either reducing J_{max} alone as in the case of the latter

714 two studies, or by decreasing J_{max} and increasing V_{cmax} simultaneously whilst keeping the total amount of leaf

715 nitrogen the same as used in the present study and in Mercado et al. (2018). The simulated response of thermal

716 acclimation therefore appears to be sensitive to this subtlety in the parameterisation of the acclimation schemes

717 and warrants further investigation. Yet a clear understanding of what drives the change in the $J_{max}:V_{cmax}$ ratio in

718 response to T_{growth} is still lacking. More recent results from the analysis by Kumarathunge et al. (2019b) highlight

719 the difficulty in pinning down what drives this process. They found that the $J_{max}:V_{cmax}$ ratio responded strongly

720 and consistently to T_{growth}, but whether that was achieved by increasing V_{cmax}, decreasing J_{max} or both was highly

721 variable.

722 The behaviour of the thermal acclimation scheme in JULES in response to long term warming implies unlimited

723 thermal resilience of vegetation, but how realistic is this? Observational studies suggest temperate tree species

724 have sufficient capacity to acclimate to rising temperatures e.g. (Drake et al., 2015; Reich et al., 2018; Sendall et

725 al., 2015), although large inter-specific variability in thermal tolerance is identified in co-occurring temperate tree

726 species (Guha et al., 2018). Studies exploring thermal acclimation of photosynthesis for grasslands and C_3

727 herbaceous vegetation are more limited. For boreal tree species, experimental studies suggest high variability

728 between species with respect to photosynthetic acclimation responses to increasing temperatures, for example,

729 there is an increasing body of work suggesting that the evergreen boreal conifer species *Picea* might be particularly

730 vulnerable to warming (Benomar et al., 2017; Dusenge et al., 2020; Kroner and Way, 2016; Kurepin et al., 2018;

731 Way and Sage, 2008; Zhang et al., 2015). The three year open-air warming experiment of Reich et al. (2018)

732 showed that for 11 temperate and boreal tree species studied, warming increased photosynthesis in most species

733 on wet soils, but not in drier conditions. Further, under moist soil conditions, all deciduous species showed an

734 acclimation response to increased temperatures, however, the two boreal evergreen species, *Abies* and *Picea*,

735 showed no thermal acclimation response at any soil moisture concentration. It is generally thought that evergreen

736 species have a reduced capacity to acclimate growth and photosynthesis to warming compared to deciduous tree

737 species (Dusenge et al., 2020; Way and Yamori, 2014). Therefore, the response of boreal forest ecosystems to

738 warming will depend on species composition given the varied acclimation capacities shown and lower diversity

739 of boreal forests, and, as Reich et al. (2018) highlight, also on interaction with other climate changes such as

740 precipitation. In contrast to temperate and boreal forests, tropical forests are thought to be more susceptible to

741 climate change, having evolved under relatively narrow temperature regimes, and experiencing less seasonal and

742 day-to-day variation in temperature changes (Cunningham and Read, 2003). As a consequence, an increasing

743 number of studies show that tropical trees have less capacity to physiologically acclimate photosynthesis to

744 increasing temperatures (Carter et al., 2021; Dusenge et al., 2021; Mau et al., 2018; Miller et al., 2021; Vårhammar

745 et al., 2015). Other studies have determined high temperature threshold responses of photosynthesis, indicating

746 an ability of tropical trees to acclimate to moderate warming, but more severe warming decreases carbon gain

747 (Doughty and Goulden, 2008; Pau et al., 2018; Slot and Winter, 2017; Sullivan et al., 2020). In two tropical

748 understorey species acclimation of the T_{opt} of photosynthesis was observed in the early successional species,

749 whereas no acclimation capacity was shown by the mid-successional species (Carter et al., 2020). Our study

750 demonstrates a large positive impact of thermal acclimation on GPP in tropical forests. However a notable

751 uncertainty in the parameterisation is that the dataset used in the Kattge and Knorr (2007) scheme to construct the

752 empirical relationships is heavily weighted towards temperate species, including only two boreal species and no

753 tropical species (Kattge and Knorr, 2007). There is a significant gap in understanding tropical forest responses to

754 increasing temperature. Observational studies are starting to address this gap, but this increasing knowledge is yet

755 to be incorporated into models. Therefore, whilst results from this study demonstrate the importance of thermal

756 acclimation of photosynthesis on simulation of the future global carbon cycle, they should be interpreted with

757 some caution. The varied results from experimental studies highlights the research needed to further understand

758 thermal acclimation responses in a variety of ecosystems, over different timescales, and from leaf-level through

759 to canopy, and finally to translate that understanding so it is amenable to incorporation into ESMs.

760 **5.2 Performance of the new JULES plant physiology model configurations: Medlyn g_s**

761 In this study, the Medlyn g_s model had the biggest impact on surface energy fluxes simulated by the C_3 grass PFT

762 and needleleaf evergreen tree PFT in JULES. This reflects a change to the water-use strategy of these PFTs as

763 reported by Lin et al. (2015) that is not currently captured by parameterisations in the JULES Jacobs model. Global

764 simulations with the Medlyn scheme for the recent contemporary period simulated a ~10% decrease in LE

765 (increased H) across the high northern latitudes dominated by the NET PFT compared to the standard JULES

766 Jacobs g_s scheme. The future climate change experiment showed a large response across the temperate region

767 dominated by the C3 PFT, where LE increased by ~30% (H decreased) with Medlyn. Our study for current-day

768 is in agreement with De Kauwe et al. (2015) who found a large impact of the Medlyn model on transpiration

769 fluxes in needle leaved evergreen trees (~30% reduction) in the CABLE LSM . Coupled simulations using CABLE

770 within the Australian Community Climate and Earth Systems Simulator (ACCESSv1.3b) showed that the Medlyn

771 g_s scheme reduced the LE flux from the land surface over the boreal forests during JJA by 0.5–1.0 mm day^{-1},

772 leading to warmer daily maximum and minimum temperatures by up to 1.0°C and warmer extreme maximum

773 temperatures by up to 1.5°C (Kala et al., 2015). In future simulations, this new parameterisation of the stomatal

774 scheme in ACCESS1.3 substantially increased the intensity of future heatwaves across Northern Eurasia (Kala et

775 al., 2016).

776 **5.3 Implications for land-atmosphere feedbacks**

777 Modifying the leaf-level stomatal behaviour in JULES impacts the simulated surface energy fluxes. In our study,

778 a change of stomatal opening results from either a direct change in the parameterisation of g_s or through altered

779 stomatal behaviour in response to temperature. In our offline climate change simulation, thermal acclimation

780 increased stomatal opening in response to long term warming, and in some regions this increased the rate of

781 transpiration and evaporative cooling, and decreased the sensible heat flux. When coupled to an atmospheric

782 model, such behaviours have potential to feed-back on the land surface via changes in temperature, cloud cover

783 and precipitation, as for example modelled by De Arellano et al. (2012); Kala et al. (2015); Kala et al. (2016);

784 Kooperman et al. (2018); Zeng et al. (2017). The extent and amplitude of acclimation-induced perturbations to

785 surface energy fluxes in our offline simulation suggests a potential impact on regional scale circulations, for

786 example across the East Asian monsoon region. The impact of these changes to the plant physiology routines in

787 JULES on land-atmosphere feedbacks will be investigated in future work through coupled simulations in the

788 HadGEM global climate model.

5.4 Limitations of this study

Across all latitudes, the changes introduced to JULES by the new plant physiology routines did not degrade the performance of JULES. All model configurations compared reasonably well to the FluxCom and MOD17 GPP products, and FluxCom and GLEAM ET products, given that there are also uncertainties inherent in estimates from these products. For example, the satellite-based products of GPP have recently been shown to incorrectly capture the response of photosynthesis to CO_2, which means they potentially underestimate the response of GPP to rising atmospheric CO_2 (Keenan et al., 2021). Nevertheless, some notable biases in the model were identified that were common to all JULES model configurations, for example the over-prediction of GPP and ET in the temperate and boreal region in SON, and the over-prediction of both fluxes in MAM in the southern tropics (0 to -20ºS). Potential sources of error to consider may be the use of a prescribed climatology of MODIS based LAI, which some studies have reported to be inaccurate over forested areas (Shabanov et al., 2005). Other processes currently missing in the model may also contribute to these large biases, such as a lack of seasonality in photosynthetic capacity (i.e. V_{cmax} and J_{max}) which has been demonstrated for many different forest species, and without which likely causes over-estimation of forest carbon exchange (Croft et al., 2017; Wilson K.B et al., 2001).

More generally, this study revealed limited data to inform the temperature sensitivity response functions of different PFTs for implementation into LSMs. We found only a few datasets for C_3 grass/herbaceous vegetation (e.g. Wohlfahrt *et al*., (1999) and Joseph *et al*., (2014)) which represents only limited geographical coverage. Consequently, we fitted the temperature response function for this PFT in the Farquhar scheme to that of the existing function in the JULES Collatz photosynthesis scheme. We also encountered an issue regarding uncertainty about the temperature response functions at low temperatures. The data-led functions we implemented for all PFTs (with the exception of the C3 PFT) from Kumarathunge et al. (2019b) showed higher rates of leaf-level photosynthesis at low leaf temperatures compared to the existing functions in the JULES Collatz scheme, where photosynthesis was much lower and goes to zero at 0 ºC for most PFTs (see PFT leaf-level temperature sensitivity curves for gross photosynthesis in Fig. S1). In our simulations this led to higher GPP in DJF when using the Farquhar scheme, which increased biases with respect to FluxCom and MOD17 global estimates of GPP. It is desirable to use the temperature response functions from Kumarathunge et al. (2019b) as these are entirely data-led. However for some PFTs the resulting behaviour of photosynthesis at very low temperatures looks potentially unrealistic, and the question here is how well constrained by observations are the temperature sensitivity curves at low temperatures? For global modelling applications, understanding the response of photosynthesis to temperature over a wide temperature range is essential, including at low temperatures as well as around the T_{opt} of photosynthesis for different species and PFTs. Additionally, increasing the understanding and data availability of the temperature sensitivity of different species from different biomes will allow greater representation within LSMs of the variation that exists across the globe.

5.5 Conclusions

Here we introduce new representations of plant physiological processes into the JULES model, building enhanced capability, and allowing stronger links between model and field studies. This work a) introduces updated understanding of plant physiological processes into JULES, b) increases the flexibility of the modelling capacity

827 within JULES by allowing use of two alternative photosynthesis and g_s schemes, in addition to thermal

828 acclimation of photosynthesis, and c) provides new parameters that are entirely based on large observational

829 datasets. Testing and evaluation at site-level and globally show some key improvements are made to the JULES

830 model. Thermal acclimation of photosynthesis coupled with the optimality-based g_s scheme led to improved

831 simulated carbon fluxes across much of the tropics for the present-day. With about 40% of the world's vegetation

832 carbon residing in tropical forests, they play a crucial role in regulating both regional and global climate through

833 water and carbon cycle dynamics (Erb et al., 2018; Pan et al., 2011). Therefore, accurate representation of tropical

834 carbon fluxes within LSMs is important. Thermal acclimation and the optimality-based g_s scheme also improved

835 simulated carbon fluxes in the high northern latitude forests in the northern hemisphere summer, and the same

836 model configuration also improved simulated water fluxes across much of this region in the same season. The

837 optimality-based Medlyn g_s scheme reduced the LE flux substantially across the northern boreal forests in JJA.

838 This change reflects a more conservative water-use strategy for the needleleaf evergreen tree PFT that dominates

839 in this region as suggested by the global synthesis of experimental data from Lin et al. (2015). The current JULES

840 Jacobs scheme parameterisation does not accurately capture the water-use strategy of this PFT. Our future climate

841 experiment highlights the impact of thermal acclimation on simulating carbon cycle dynamics and energy fluxes

842 in response to long-term warming. The potential impact of this altered stomatal behaviour on land-atmosphere

843 feedbacks via changes in surface energy fluxes will be examined in future coupled simulations.

844

Code/Data availability

846 JULES-vn5.6 was used for all simulations. The JULES model code and suites used to run the model are available

847 from the Met Office Science Repository Service (MOSRS). Registration is required and code is freely available

848 to anyone for non-commercial use (see here for details of licensing https://jules.jchmr.org/content/code). Visit the

849 JULES website (https://jules.jchmr.org/content/getting-started) to register for a MOSRS account. The results

850 presented in this paper were obtained by running JULES from the following branch:

851 https://code.metoffice.gov.uk/trac/jules/browser/main/branches/dev/douglasclark/vn5.6_acclimation@16578.

852 This is a development branch of JULES-vn5.6 to include thermal acclimation of photosynthesis as described in

853 this paper. This branch can be accessed and downloaded from the Met Office Science Repository Service once

854 the user has registered for an account, as outlined above. Documentation for the JULES model is located here:

855 https://jules-lsm.github.io/vn5.6/. Output data from the model simulations, and R scripts to produce the plots in

856 the paper are provided at (https://doi.org/10.5281/zenodo.5825540). Site-level simulations used the rose suite u-

857 br064 (https://code.metoffice.gov.uk/trac/roses-u/browser/b/r/0/6/4/ at revision 146216) which is a copy of the u-

858 al752 JULES suite for FLUXNET 2015 and LBA sites described here

859 https://code.metoffice.gov.uk/trac/jules/wiki/FluxnetandLbaSites, and downloaded from here

860 https://code.metoffice.gov.uk/trac/roses-u/browser/a/l/7/5/2/ at revision 145397). The global simulations used

861 JULES rose suite u-bq898 (https://code.metoffice.gov.uk/trac/roses-u/browser/b/q/8/9/8/ at revision 181188)

862 which uses the Global Land configuration 7.1 (Wiltshire et al., 2020). Suites can be downloaded from MOSRS

863 once the user has registered for an account.

864

Competing Interests

Author Contributions

868   RJO performed simulations and analysis and wrote the first version of the manuscript. DBC, LMM and RJO
869   developed the model. PLV, PCM and MT provided data for the future climate runs, help with developing the
870   JULES suites, and general expertise. CH assisted with analysis. SF and SS provided ancillary data for forcing the
871   model. LMM, CMT, CH, PLV, BEM, PCM and MT contributed to editing the manuscript. All authors contributed
872   to discussions throughout to develop the work.

873
874

875   **Acknowledgements**

876   This work and its contributors (RJO, LMM, CH, CMT, PLV, PCM, MT and SF) were supported by the UK-China
877   Research & Innovation Partnership Fund through the Met Office Climate Science for Service Partnership (CSSP)
878   China as part of the Newton Fund. R.J.O. acknowledges support from the Natural Environment Research Council,
879   grant NEC05816 LTS-M-UKESM. This work used eddy covariance data acquired and shared by the FLUXNET
880   community, including these networks: AmeriFlux, AfriFlux, AsiaFlux, CarboAfrica, CarboEuropeIP, CarboItaly,
881   CarboMont, ChinaFlux, Fluxnet-Canada, GreenGrass, ICOS, KoFlux, LBA, NECC, OzFlux-TERN, TCOS-
882   Siberia and USCCC. The ERA-Interim reanalysis data are provided by ECMWF and processed by LSCE. The
883   FLUXNET eddy covariance data processing and harmonization was carried out by the European Fluxes Database
884   Cluster, AmeriFlux Management Project, and Fluxdata project of FLUXNET, with the support of CDIAC and
885   ICOS Ecosystem Thematic Center, and the OzFlux, ChinaFlux and AsiaFlux offices.

886

887

888

889

890   **References**

891

892   Atkin, O. K., Scheurwater, I., and Pons, T. L.: High thermal acclimation potential of both photosynthesis and
893   respiration in two lowland Plantago species in contrast to an alpine congeneric, Global Change Biology, 12, 500-
894   515, https://doi.org/10.1111/j.1365-2486.2006.01114.x, 2006.

895   Ball, M. C., Woodrow, I. E., and Berry, J. A.: A model predicting stomatal conductance and its contribution to
896   the control of photosynthesis under different environmental conditions. , In Progress in Photosynthesis Research
897   (ed J. Biggins). Martinus Nijhoff Publishers, Dordrecht, Netherlands., 221-224, 1987.

898   Benomar, L., Lamhamedi, M. S., Pepin, S., Rainville, A., Lambert, M.-C., Margolis, H. A., Bousquet, J., and
899   Beaulieu, J.: Thermal acclimation of photosynthesis and respiration of southern and northern white spruce seed

900   sources tested along a regional climatic gradient indicates limited potential to cope with temperature warming,
901   Annals of Botany, 121, 443-457, 10.1093/aob/mcx174, 2017.

902   Bernacchi, C. J., Singsaas, E. L., Pimentel, C., Portis Jr, A. R., and Long, S. P.: Improved temperature response
903   functions for models of Rubisco-limited photosynthesis, Plant, Cell & Environment, 24, 253-259,
904   https://doi.org/10.1111/j.1365-3040.2001.00668.x, 2001.

905   Best, M. J., Pryor, M., Clark, D. B., Rooney, G. G., Essery, R. L. H., Ménard, C. B., Edwards, J. M., Hendry, M.
906   A., Porson, A., Gedney, N., Mercado, L. M., Sitch, S., Blyth, E., Boucher, O., Cox, P. M., Grimmond, C. S. B.,
907   and Harding, R. J.: The Joint UK Land Environment Simulator (JULES), model description – Part 1: Energy and
908   water fluxes, Geosci. Model Dev., 4, 677-699, 10.5194/gmd-4-677-2011, 2011.

909   Betts, R. A., Boucher, O., Collins, M., Cox, P. M., Falloon, P. D., Gedney, N., Hemming, D. L., Huntingford, C.,
910   Jones, C. D., Sexton, D. M. H., and Webb, M. J.: Projected increase in continental runoff due to plant responses
911   to increasing carbon dioxide, Nature, 448, 1037-1041, 10.1038/nature06045, 2007.

912   Booth, B. B. B., Jones, C. D., Collins, M., Totterdell, I. J., Cox, P. M., Sitch, S., Huntingford, C., Betts, R. A.,
913   Harris, G. R., and Lloyd, J.: High sensitivity of future global warming to land carbon cycle processes,
914   Environmental Research Letters, 7, 024002, 10.1088/1748-9326/7/2/024002, 2012.

915   Carter, K. R., Wood, T. E., Reed, S. C., Butts, K. M., and Cavaleri, M. A.: Experimental warming across a tropical
916   forest canopy height gradient reveals minimal photosynthetic and respiratory acclimation, Plant, Cell &
917   Environment, 44, 2879-2897, https://doi.org/10.1111/pce.14134, 2021.

918   Carter, K. R., Wood, T. E., Reed, S. C., Schwartz, E. C., Reinsel, M. B., Yang, X., and Cavaleri, M. A.:
919   Photosynthetic and Respiratory Acclimation of Understory Shrubs in Response to in situ Experimental Warming
920   of a Wet Tropical Forest, Frontiers in Forests and Global Change, 3, 10.3389/ffgc.2020.576320, 2020.

921   Chen, M. I. N. and Zhuang, Q.: Modelling temperature acclimation effects on the carbon dynamics of forest
922   ecosystems in the conterminous United States, Tellus B: Chemical and Physical Meteorology, 65, 19156,
923   10.3402/tellusb.v65i0.19156, 2013.

924   Clark, D. B., Mercado, L. M., Sitch, S., Jones, C. D., Gedney, N., Best, M. J., Pryor, M., Rooney, G. G., Essery,
925   R. L. H., Blyth, E., Boucher, O., Harding, R. J., Huntingford, C., and Cox, P. M.: The Joint UK Land Environment
926   Simulator (JULES), model description – Part 2: Carbon fluxes and vegetation dynamics, Geosci. Model Dev., 4,
927   701-722, 10.5194/gmd-4-701-2011, 2011.

928   Collatz, G., Ribas-Carbo, M., and Berry, J.: Coupled Photosynthesis-Stomatal Conductance Model for Leaves of
929   C_4 Plants, Functional Plant Biology, 19, 519-538, https://doi.org/10.1071/PP9920519, 1992.

930   Collatz, G. J., Ball, J. T., Grivet, C., and Berry, J. A.: Physiological and environmental regulation of stomatal
931   conductance, photosynthesis and transpiration: a model that includes a laminar boundary layer, Agricultural and
932   Forest Meteorology, 54, 107-136, https://doi.org/10.1016/0168-1923(91)90002-8, 1991.

933   Cox, P. M., Huntingford, C., and Harding, R. J.: A canopy conductance and photosynthesis model for use in a
934   GCM land surface scheme, Journal of Hydrology, 212-213, 79-94, https://doi.org/10.1016/S0022-
935   1694(98)00203-0, 1998.

936   Croft, H., Chen, J. M., Luo, X., Bartlett, P., Chen, B., and Staebler, R. M.: Leaf chlorophyll content as a proxy for
937   leaf photosynthetic capacity, Global Change Biology, 23, 3513-3524, https://doi.org/10.1111/gcb.13599, 2017.

938   Cruz, F. T., Pitman, A. J., and Wang, Y. P.: Can the stomatal response to higher atmospheric carbon dioxide
939   explain the unusual temperatures during the 2002 Murray-Darling Basin drought?, Journal of Geophysical
940   Research: Atmospheres, 115, https://doi.org/10.1029/2009JD012767, 2010.

941   Cunningham, S. C. and Read, J.: Do temperate rainforest trees have a greater ability to acclimate to changing
942   temperatures than tropical rainforest trees?, New Phytologist, 157, 55-64, https://doi.org/10.1046/j.1469-
943   8137.2003.00652.x, 2003.

944   Damour, G., Simonneau, T., Cochard, H., and Urban, L.: An overview of models of stomatal conductance at the
945   leaf level, Plant, Cell & Environment, 33, 1419-1438, https://doi.org/10.1111/j.1365-3040.2010.02181.x, 2010.

946   de Arellano, J. V.-G., van Heerwaarden, C. C., and Lelieveld, J.: Modelled suppression of boundary-layer clouds
947   by plants in a CO2-rich atmosphere, Nature Geoscience, 5, 701-704, 10.1038/ngeo1554, 2012.

948   De Kauwe, M. G., Kala, J., Lin, Y. S., Pitman, A. J., Medlyn, B. E., Duursma, R. A., Abramowitz, G., Wang, Y.
949   P., and Miralles, D. G.: A test of an optimal stomatal conductance scheme within the CABLE land surface model,
950   Geosci. Model Dev., 8, 431-452, 10.5194/gmd-8-431-2015, 2015.

951   De Kauwe, M. G., Medlyn, B. E., Zaehle, S., Walker, A. P., Dietze, M. C., Hickler, T., Jain, A. K., Luo, Y.,
952   Parton, W. J., Prentice, I. C., Smith, B., Thornton, P. E., Wang, S., Wang, Y.-P., Wårlind, D., Weng, E., Crous,
953   K. Y., Ellsworth, D. S., Hanson, P. J., Seok Kim, H.-., Warren, J. M., Oren, R., and Norby, R. J.: Forest water use
954   and water use efficiency at elevated CO2: a model-data intercomparison at two contrasting temperate forest FACE
955   sites, Global Change Biology, 19, 1759-1779, https://doi.org/10.1111/gcb.12164, 2013.

956   Doughty, C. E. and Goulden, M. L.: Are tropical forests near a high temperature threshold?, Journal of
957   Geophysical Research: Biogeosciences, 113, https://doi.org/10.1029/2007JG000632, 2008.

958   Drake, J. E., Aspinwall, M. J., Pfautsch, S., Rymer, P. D., Reich, P. B., Smith, R. A., Crous, K. Y., Tissue, D. T.,
959   Ghannoum, O., and Tjoelker, M. G.: The capacity to cope with climate warming declines from temperate to
960   tropical latitudes in two widely distributed Eucalyptus species, Global Change Biology, 21, 459-472,
961   https://doi.org/10.1111/gcb.12729, 2015.

962   Dusenge, M. E., Madhavji, S., and Way, D. A.: Contrasting acclimation responses to elevated CO2 and warming
963   between an evergreen and a deciduous boreal conifer, Global Change Biology, 26, 3639-3657,
964   https://doi.org/10.1111/gcb.15084, 2020.

965   Dusenge, M. E., Wittemann, M., Mujawamariya, M., Ntawuhiganayo, E. B., Zibera, E., Ntirugulirwa, B., Way,
966   D. A., Nsabimana, D., Uddling, J., and Wallin, G.: Limited thermal acclimation of photosynthesis in tropical
967   montane tree species, Global Change Biology, 27, 4860-4878, https://doi.org/10.1111/gcb.15790, 2021.

968   Erb, K.-H., Kastner, T., Plutzar, C., Bais, A. L. S., Carvalhais, N., Fetzel, T., Gingrich, S., Haberl, H., Lauk, C.,
969   Niedertscheider, M., Pongratz, J., Thurner, M., and Luyssaert, S.: Unexpectedly large impact of forest
970   management and grazing on global vegetation biomass, Nature, 553, 73-76, 10.1038/nature25138, 2018.

971   Eyring, V., Bony, S., Meehl, G. A., Senior, C. A., Stevens, B., Stouffer, R. J., and Taylor, K. E.: Overview of the
972   Coupled Model Intercomparison Project Phase 6 (CMIP6) experimental design and organization, Geosci. Model
973   Dev., 9, 1937-1958, 10.5194/gmd-9-1937-2016, 2016.

974   Farquhar, G. D., von Caemmerer, S., and Berry, J. A.: A biochemical model of photosynthetic CO_2 assimilation
975   in leaves of C3 species, Planta, 149, 78-90, 10.1007/BF00386231, 1980.

976   Franks, P. J., Berry, J. A., Lombardozzi, D. L., and Bonan, G. B.: Stomatal Function across Temporal and Spatial
977   Scales: Deep-Time Trends, Land-Atmosphere Coupling and Global Models, Plant Physiology, 174, 583-602,
978   10.1104/pp.17.00287, 2017.

979   Franks, P. J., Bonan, G. B., Berry, J. A., Lombardozzi, D. L., Holbrook, N. M., Herold, N., and Oleson, K. W.:
980   Comparing optimal and empirical stomatal conductance models for application in Earth system models, Global
981   Change Biology, 24, 5708-5723, https://doi.org/10.1111/gcb.14445, 2018.

982   Friedlingstein, P., Meinshausen, M., Arora, V. K., Jones, C. D., Anav, A., Liddicoat, S. K., and Knutti, R.:
983   Uncertainties in CMIP5 Climate Projections due to Carbon Cycle Feedbacks, Journal of Climate, 27, 511-526,
984   10.1175/jcli-d-12-00579.1, 2014.

985   Friedlingstein, P., O'Sullivan, M., Jones, M. W., Andrew, R. M., Hauck, J., Olsen, A., Peters, G. P., Peters, W.,
986   Pongratz, J., Sitch, S., Le Quéré, C., Canadell, J. G., Ciais, P., Jackson, R. B., Alin, S., Aragão, L. E. O. C., Arneth,
987   A., Arora, V., Bates, N. R., Becker, M., Benoit-Cattin, A., Bittig, H. C., Bopp, L., Bultan, S., Chandra, N.,
988   Chevallier, F., Chini, L. P., Evans, W., Florentie, L., Forster, P. M., Gasser, T., Gehlen, M., Gilfillan, D.,
989   Gkritzalis, T., Gregor, L., Gruber, N., Harris, I., Hartung, K., Haverd, V., Houghton, R. A., Ilyina, T., Jain, A. K.,
990   Joetzjer, E., Kadono, K., Kato, E., Kitidis, V., Korsbakken, J. I., Landschützer, P., Lefèvre, N., Lenton, A., Lienert,
991   S., Liu, Z., Lombardozzi, D., Marland, G., Metzl, N., Munro, D. R., Nabel, J. E. M. S., Nakaoka, S. I., Niwa, Y.,
992   O'Brien, K., Ono, T., Palmer, P. I., Pierrot, D., Poulter, B., Resplandy, L., Robertson, E., Rödenbeck, C.,
993   Schwinger, J., Séférian, R., Skjelvan, I., Smith, A. J. P., Sutton, A. J., Tanhua, T., Tans, P. P., Tian, H., Tilbrook,
994   B., van der Werf, G., Vuichard, N., Walker, A. P., Wanninkhof, R., Watson, A. J., Willis, D., Wiltshire, A. J.,
995   Yuan, W., Yue, X., and Zaehle, S.: Global Carbon Budget 2020, Earth Syst. Sci. Data, 12, 3269-3340,
996   10.5194/essd-12-3269-2020, 2020.

997   Gedney, N., Cox, P. M., Betts, R. A., Boucher, O., Huntingford, C., and Stott, P. A.: Detection of a direct carbon
998   dioxide effect in continental river runoff records, Nature, 439, 835-838, 10.1038/nature04504, 2006.

999   Guha, A., Han, J., Cummings, C., McLennan, D. A., and Warren, J. M.: Differential ecophysiological responses
1000   and resilience to heat wave events in four co-occurring temperate tree species, Environmental Research Letters,
1001   13, 065008, 10.1088/1748-9326/aabcd8, 2018.

1002 Gunderson, C. A., Norby, R. J., and Wullschleger, S. D.: Acclimation of photosynthesis and respiration to
1003 simulated climatic warming in northern and southern populations of Acer saccharum: laboratory and field
1004 evidence, Tree Physiology, 20, 87-96, 10.1093/treephys/20.2.87, 2000.

1005 Gunderson, C. A., O'Hara, K. H., Campion, C. M., Walker, A. V., and Edwards, N. T.: Thermal plasticity of
1006 photosynthesis: the role of acclimation in forest responses to a warming climate, Global Change Biology, 16,
1007 2272-2286, https://doi.org/10.1111/j.1365-2486.2009.02090.x, 2010.

1008 Haarsma, R. J., Roberts, M. J., Vidale, P. L., Senior, C. A., Bellucci, A., Bao, Q., Chang, P., Corti, S., Fučkar, N.
1009 S., Guemas, V., von Hardenberg, J., Hazeleger, W., Kodama, C., Koenigk, T., Leung, L. R., Lu, J., Luo, J. J.,
1010 Mao, J., Mizielinski, M. S., Mizuta, R., Nobre, P., Satoh, M., Scoccimarro, E., Semmler, T., Small, J., and von
1011 Storch, J. S.: High Resolution Model Intercomparison Project (HighResMIP v1.0) for CMIP6, Geosci. Model
1012 Dev., 9, 4185-4208, 10.5194/gmd-9-4185-2016, 2016.

1013 Harper, A. B., Cox, P. M., Friedlingstein, P., Wiltshire, A. J., Jones, C. D., Sitch, S., Mercado, L. M., Groenendijk,
1014 M., Robertson, E., Kattge, J., Bönisch, G., Atkin, O. K., Bahn, M., Cornelissen, J., Niinemets, Ü., Onipchenko,
1015 V., Peñuelas, J., Poorter, L., Reich, P. B., Soudzilovskaia, N. A., and Bodegom, P. V.: Improved representation
1016 of plant functional types and physiology in the Joint UK Land Environment Simulator (JULES v4.2) using plant
1017 trait information, Geosci. Model Dev., 9, 2415-2440, 10.5194/gmd-9-2415-2016, 2016.

1018 Hernández, G. G., Winter, K., and Slot, M.: Similar temperature dependence of photosynthetic parameters in sun
1019 and shade leaves of three tropical tree species, Tree Physiology, 40, 637-651, 10.1093/treephys/tpaa015, 2020.

1020 Hikosaka, K., Nabeshima, E., and Hiura, T.: Seasonal changes in the temperature response of photosynthesis in
1021 canopy leaves of Quercus crispula in a cool-temperate forest, Tree Physiology, 27, 1035-1041,
1022 10.1093/treephys/27.7.1035, 2007.

1023 Huntingford, C. and Oliver, R. J.: Converging towards a common representation of large-scale photosynthesis,
1024 Global Change Biology, 27, 716-718, https://doi.org/10.1111/gcb.15398, 2021.

1025 Huntingford, C., Lowe, J. A., Booth, B. B. B., Jones, C. D., Harris, G. R., Gohar, L. K., and Meir, P.: Contributions
1026 of carbon cycle uncertainty to future climate projection spread, Tellus B: Chemical and Physical Meteorology,
1027 61, 355-360, 10.1111/j.1600-0889.2008.00414.x, 2009.

1028 Jacobs, C. M. J.: Direct impact of atmospheric CO2 enrichment on regional transpiration, Jacobs, S.l., 1994.

1029 Jarvis, P. G., Monteith, J. L., and Weatherley, P. E.: The interpretation of the variations in leaf water potential and
1030 stomatal conductance found in canopies in the field, Philosophical Transactions of the Royal Society of London.
1031 B, Biological Sciences, 273, 593-610, doi:10.1098/rstb.1976.0035, 1976.

1032 Jasechko, S., Sharp, Z. D., Gibson, J. J., Birks, S. J., Yi, Y., and Fawcett, P. J.: Terrestrial water fluxes dominated
1033 by transpiration, Nature, 496, 347-350, 10.1038/nature11983, 2013.

1034 Joseph, T., Whitehead, D., and Turnbull, M. H.: Soil water availability influences the temperature response of
1035 photosynthesis and respiration in a grass and a woody shrub, Functional Plant Biology, 41, 468-481,
1036 https://doi.org/10.1071/FP13237, 2014.

1037   Jung, M., Koirala, S., Weber, U., Ichii, K., Gans, F., Camps-Valls, G., Papale, D., Schwalm, C., Tramontana, G.,
1038   and Reichstein, M.: The FLUXCOM ensemble of global land-atmosphere energy fluxes, Scientific Data, 6, 74,
1039   10.1038/s41597-019-0076-8, 2019.

1040   Jung, M., Schwalm, C., Migliavacca, M., Walther, S., Camps-Valls, G., Koirala, S., Anthoni, P., Besnard, S.,
1041   Bodesheim, P., Carvalhais, N., Chevallier, F., Gans, F., Goll, D. S., Haverd, V., Köhler, P., Ichii, K., Jain, A. K.,
1042   Liu, J., Lombardozzi, D., Nabel, J. E. M. S., Nelson, J. A., O'Sullivan, M., Pallandt, M., Papale, D., Peters, W.,
1043   Pongratz, J., Rödenbeck, C., Sitch, S., Tramontana, G., Walker, A., Weber, U., and Reichstein, M.: Scaling carbon
1044   fluxes from eddy covariance sites to globe: synthesis and evaluation of the FLUXCOM approach, Biogeosciences,
1045   17, 1343-1365, 10.5194/bg-17-1343-2020, 2020.

1046   Kala, J., De Kauwe, M. G., Pitman, A. J., Medlyn, B. E., Wang, Y.-P., Lorenz, R., and Perkins-Kirkpatrick, S. E.:
1047   Impact of the representation of stomatal conductance on model projections of heatwave intensity, Scientific
1048   Reports, 6, 23418, 10.1038/srep23418, 2016.

1049   Kala, J., De Kauwe, M. G., Pitman, A. J., Lorenz, R., Medlyn, B. E., Wang, Y. P., Lin, Y. S., and Abramowitz,
1050   G.: Implementation of an optimal stomatal conductance scheme in the Australian Community Climate Earth
1051   Systems Simulator (ACCESS1.3b), Geosci. Model Dev., 8, 3877-3889, 10.5194/gmd-8-3877-2015, 2015.

1052   Kattge, J. and Knorr, W.: Temperature acclimation in a biochemical model of photosynthesis: a reanalysis of data
1053   from 36 species, Plant, Cell & Environment, 30, 1176-1190, 10.1111/j.1365-3040.2007.01690.x, 2007.

1054   Keenan, T. F., Luo, X., De Kauwe, M. G., Medlyn, B. E., Prentice, I. C., Stocker, B. D., Smith, N. G., Terrer, C.,
1055   Wang, H., Zhang, Y., and Zhou, S.: A constraint on historic growth in global photosynthesis due to increasing
1056   CO2, Nature, 600, 253-258, 10.1038/s41586-021-04096-9, 2021.

1057   Kooperman, G. J., Chen, Y., Hoffman, F. M., Koven, C. D., Lindsay, K., Pritchard, M. S., Swann, A. L. S., and
1058   Randerson, J. T.: Forest response to rising CO2 drives zonally asymmetric rainfall change over tropical land,
1059   Nature Climate Change, 8, 434-440, 10.1038/s41558-018-0144-7, 2018.

1060   Krinner, G., Viovy, N., de Noblet-Ducoudré, N., Ogée, J., Polcher, J., Friedlingstein, P., Ciais, P., Sitch, S., and
1061   Prentice, I. C.: A dynamic global vegetation model for studies of the coupled atmosphere-biosphere system,
1062   Global Biogeochemical Cycles, 19, https://doi.org/10.1029/2003GB002199, 2005.

1063   Kroner, Y. and Way, D. A.: Carbon fluxes acclimate more strongly to elevated growth temperatures than to
1064   elevated CO2 concentrations in a northern conifer, Global Change Biology, 22, 2913-2928,
1065   https://doi.org/10.1111/gcb.13215, 2016.

1066   Kumarathunge, D. P., Medlyn, B. E., Drake, J. E., Rogers, A., and Tjoelker, M. G.: No evidence for triose
1067   phosphate limitation of light-saturated leaf photosynthesis under current atmospheric CO2 concentration, Plant,
1068   Cell & Environment, 42, 3241-3252, https://doi.org/10.1111/pce.13639, 2019a.

1069   Kumarathunge, D. P., Medlyn, B. E., Drake, J. E., Tjoelker, M. G., Aspinwall, M. J., Battaglia, M., Cano, F. J.,
1070   Carter, K. R., Cavaleri, M. A., Cernusak, L. A., Chambers, J. Q., Crous, K. Y., De Kauwe, M. G., Dillaway, D.
1071   N., Dreyer, E., Ellsworth, D. S., Ghannoum, O., Han, Q., Hikosaka, K., Jensen, A. M., Kelly, J. W. G., Kruger,
1072   E. L., Mercado, L. M., Onoda, Y., Reich, P. B., Rogers, A., Slot, M., Smith, N. G., Tarvainen, L., Tissue, D. T.,

1073   Togashi, H. F., Tribuzy, E. S., Uddling, J., Vårhammar, A., Wallin, G., Warren, J. M., and Way, D. A.:
1074   Acclimation and adaptation components of the temperature dependence of plant photosynthesis at the global scale,
1075   New Phytologist, 222, 768-784, https://doi.org/10.1111/nph.15668, 2019b.

1076   Kurepin, L. V., Stangl, Z. R., Ivanov, A. G., Bui, V., Mema, M., Hüner, N. P. A., Öquist, G., Way, D., and Hurry,
1077   V.: Contrasting acclimation abilities of two dominant boreal conifers to elevated CO2 and temperature, Plant, Cell
1078   & Environment, 41, 1331-1345, https://doi.org/10.1111/pce.13158, 2018.

1079   Leuning, R.: A critical appraisal of a combined stomatal-photosynthesis model for C3 plants, Plant, Cell &
1080   Environment, 18, 339-355, https://doi.org/10.1111/j.1365-3040.1995.tb00370.x, 1995.

1081   Lin, Y.-S., Medlyn, B. E., Duursma, R. A., Prentice, I. C., Wang, H., Baig, S., Eamus, D., de Dios, Victor R.,
1082   Mitchell, P., Ellsworth, D. S., de Beeck, M. O., Wallin, G., Uddling, J., Tarvainen, L., Linderson, M.-L., Cernusak,
1083   L. A., Nippert, J. B., Ocheltree, T. W., Tissue, D. T., Martin-StPaul, N. K., Rogers, A., Warren, J. M., De Angelis,
1084   P., Hikosaka, K., Han, Q., Onoda, Y., Gimeno, T. E., Barton, C. V. M., Bennie, J., Bonal, D., Bosc, A., Löw, M.,
1085   Macinins-Ng, C., Rey, A., Rowland, L., Setterfield, S. A., Tausz-Posch, S., Zaragoza-Castells, J., Broadmeadow,
1086   M. S. J., Drake, J. E., Freeman, M., Ghannoum, O., Hutley, Lindsay B., Kelly, J. W., Kikuzawa, K., Kolari, P.,
1087   Koyama, K., Limousin, J.-M., Meir, P., Lola da Costa, A. C., Mikkelsen, T. N., Salinas, N., Sun, W., and Wingate,
1088   L.: Optimal stomatal behaviour around the world, Nature Climate Change, 5, 459-464, 10.1038/nclimate2550,
1089   2015.

1090   Liu, H., Randerson, J. T., Lindfors, J., Massman, W. J., and Foken, T.: Consequences of Incomplete Surface
1091   Energy Balance Closure for CO2 Fluxes from Open-Path CO2/H2O Infrared Gas Analysers, Boundary-Layer
1092   Meteorology, 120, 65-85, 10.1007/s10546-005-9047-z, 2006.

1093   Lombardozzi, D. L., Bonan, G. B., Smith, N. G., Dukes, J. S., and Fisher, R. A.: Temperature acclimation of
1094   photosynthesis and respiration: A key uncertainty in the carbon cycle-climate feedback, Geophysical Research
1095   Letters, 42, 8624-8631, https://doi.org/10.1002/2015GL065934, 2015.

1096   Mau, A. C., Reed, S. C., Wood, T. E., and Cavaleri, M. A.: Temperate and Tropical Forest Canopies are Already
1097   Functioning beyond Their Thermal Thresholds for Photosynthesis, Forests, 9, 47, 2018.

1098   Medlyn, B. E., Loustau, D., and Delzon, S.: Temperature response of parameters of a biochemically based model
1099   of photosynthesis. I. Seasonal changes in mature maritime pine (Pinus pinaster Ait.), Plant, Cell & Environment,
1100   25, 1155-1165, https://doi.org/10.1046/j.1365-3040.2002.00890.x, 2002.

1101   Medlyn, B. E., Duursma, R. A., Eamus, D., Ellsworth, D. S., Prentice, I. C., Barton, C. V. M., Crous, K. Y., de
1102   Angelis, P., Freeman, M., and Wingate, L.: Reconciling the optimal and empirical approaches to modelling
1103   stomatal   conductance,   Global   Change   Biology,   17,   2134-2144,   https://doi.org/10.1111/j.1365-
1104   2486.2010.02375.x, 2011.

1105   Mercado, L. M., Bellouin, N., Sitch, S., Boucher, O., Huntingford, C., Wild, M., and Cox, P. M.: Impact of
1106   changes in diffuse radiation on the global land carbon sink, Nature, 458, 1014-1017, 10.1038/nature07949, 2009.

1107   Mercado, L. M., Medlyn, B. E., Huntingford, C., Oliver, R. J., Clark, D. B., Sitch, S., Zelazowski, P., Kattge, J.,
1108   Harper, A. B., and Cox, P. M.: Large sensitivity in land carbon storage due to geographical and temporal variation

1109   in the thermal response of photosynthetic capacity, New Phytologist, 218, 1462-1477,
1110   https://doi.org/10.1111/nph.15100, 2018.

1111   Miller, B. D., Carter, K. R., Reed, S. C., Wood, T. E., and Cavaleri, M. A.: Only sun-lit leaves of the uppermost
1112   canopy exceed both air temperature and photosynthetic thermal optima in a wet tropical forest, Agricultural and
1113   Forest Meteorology, 301-302, 108347, https://doi.org/10.1016/j.agrformet.2021.108347, 2021.

1114   Oliver, R. J., Mercado, L. M., Sitch, S., Simpson, D., Medlyn, B. E., Lin, Y. S., and Folberth, G. A.: Large but
1115   decreasing effect of ozone on the European carbon sink, Biogeosciences, 15, 4245-4269, 10.5194/bg-15-4245-
1116   2018, 2018.

1117   Pan, Y., Birdsey, R. A., Fang, J., Houghton, R., Kauppi, P. E., Kurz, W. A., Phillips, O. L., Shvidenko, A., Lewis,
1118   S. L., Canadell, J. G., Ciais, P., Jackson, R. B., Pacala, S. W., McGuire, A. D., Piao, S., Rautiainen, A., Sitch, S.,
1119   and Hayes, D.: A Large and Persistent Carbon Sink in the World's Forests, Science, 333, 988-993,
1120   10.1126/science.1201609, 2011.

1121   Pau, S., Detto, M., Kim, Y., and Still, C. J.: Tropical forest temperature thresholds for gross primary productivity,
1122   Ecosphere, 9, e02311, https://doi.org/10.1002/ecs2.2311, 2018.

1123   Poulter, B., MacBean, N., Hartley, A., Khlystova, I., Arino, O., Betts, R., Bontemps, S., Boettcher, M.,
1124   Brockmann, C., Defourny, P., Hagemann, S., Herold, M., Kirches, G., Lamarche, C., Lederer, D., Ottlé, C., Peters,
1125   M., and Peylin, P.: Plant functional type classification for earth system models: results from the European Space
1126   Agency's Land Cover Climate Change Initiative, Geosci. Model Dev., 8, 2315-2328, 10.5194/gmd-8-2315-2015,
1127   2015.

1128   Reich, P. B., Sendall, K. M., Stefanski, A., Rich, R. L., Hobbie, S. E., and Montgomery, R. A.: Effects of climate
1129   warming on photosynthesis in boreal tree species depend on soil moisture, Nature, 562, 263-267, 10.1038/s41586-
1130   018-0582-4, 2018.

1131   Roberts, M. J., Baker, A., Blockley, E. W., Calvert, D., Coward, A., Hewitt, H. T., Jackson, L. C., Kuhlbrodt, T.,
1132   Mathiot, P., Roberts, C. D., Schiemann, R., Seddon, J., Vannière, B., and Vidale, P. L.: Description of the
1133   resolution hierarchy of the global coupled HadGEM3-GC3.1 model as used in CMIP6 HighResMIP experiments,
1134   Geosci. Model Dev., 12, 4999-5028, 10.5194/gmd-12-4999-2019, 2019.

1135   Rogers, A., Kumarathunge, D. P., Lombardozzi, D. L., Medlyn, B. E., Serbin, S. P., and Walker, A. P.: Triose
1136   phosphate utilization limitation: an unnecessary complexity in terrestrial biosphere model representation of
1137   photosynthesis, New Phytologist, 230, 17-22, https://doi.org/10.1111/nph.17092, 2021.

1138   Rogers, A., Medlyn, B. E., Dukes, J. S., Bonan, G., von Caemmerer, S., Dietze, M. C., Kattge, J., Leakey, A. D.
1139   B., Mercado, L. M., Niinemets, Ü., Prentice, I. C., Serbin, S. P., Sitch, S., Way, D. A., and Zaehle, S.: A roadmap
1140   for improving the representation of photosynthesis in Earth system models, New Phytologist, 213, 22-42,
1141   https://doi.org/10.1111/nph.14283, 2017.

1142   Schlesinger, W. H. and Jasechko, S.: Transpiration in the global water cycle, Agricultural and Forest Meteorology,
1143   189-190, 115-117, https://doi.org/10.1016/j.agrformet.2014.01.011, 2014.

1144   Sellar, A. A., Jones, C. G., Mulcahy, J. P., Tang, Y., Yool, A., Wiltshire, A., O'Connor, F. M., Stringer, M., Hill,

1145   R., Palmieri, J., Woodward, S., de Mora, L., Kuhlbrodt, T., Rumbold, S. T., Kelley, D. I., Ellis, R., Johnson, C.

1146   E., Walton, J., Abraham, N. L., Andrews, M. B., Andrews, T., Archibald, A. T., Berthou, S., Burke, E., Blockley,

1147   E., Carslaw, K., Dalvi, M., Edwards, J., Folberth, G. A., Gedney, N., Griffiths, P. T., Harper, A. B., Hendry, M.

1148   A., Hewitt, A. J., Johnson, B., Jones, A., Jones, C. D., Keeble, J., Liddicoat, S., Morgenstern, O., Parker, R. J.,

1149   Predoi, V., Robertson, E., Siahaan, A., Smith, R. S., Swaminathan, R., Woodhouse, M. T., Zeng, G., and

1150   Zerroukat, M.: UKESM1: Description and Evaluation of the U.K. Earth System Model, Journal of Advances in

1151   Modeling Earth Systems, 11, 4513-4558, https://doi.org/10.1029/2019MS001739, 2019.

1152   Sendall, K. M., Reich, P. B., Zhao, C., Jihua, H., Wei, X., Stefanski, A., Rice, K., Rich, R. L., and Montgomery,

1153   R. A.: Acclimation of photosynthetic temperature optima of temperate and boreal tree species in response to

1154   experimental forest warming, Global Change Biology, 21, 1342-1357, https://doi.org/10.1111/gcb.12781, 2015.

1155   Shabanov, N., Huang, D., Yang, W., Tan, B., Knyazikhin, Y., Myneni, R., Ahl, D., Gower, S., Huete, A., Aragao,

1156   L., and Shimabukuro, Y.: Analysis and Optimization of the MODIS Leaf Area Index Algorithm Retrievals Over

1157   Broadleaf Forests, IEEE T. Geosci. Remote, 43, 1855–1865, doi:10.1109/TGRS.2005.852477, 2005.

1158   Slot, M. and Winter, K.: Photosynthetic acclimation to warming in tropical forest tree seedlings, Journal of

1159   Experimental Botany, 68, 2275-2284, 10.1093/jxb/erx071, 2017.

1160   Slot, M., Rifai, S. W., and Winter, K.: Photosynthetic plasticity of a tropical tree species, Tabebuia rosea, in

1161   response to elevated temperature and [CO2], Plant, Cell & Environment, n/a, https://doi.org/10.1111/pce.14049,

1162   2021.

1163   Smith, N. G. and Dukes, J. S.: Plant respiration and photosynthesis in global-scale models: incorporating

1164   acclimation to temperature and CO2, Global Change Biology, 19, 45-63, https://doi.org/10.1111/j.1365-

1165   2486.2012.02797.x, 2013.

1166   Smith, N. G., Malyshev, S. L., Shevliakova, E., Kattge, J., and Dukes, J. S.: Foliar temperature acclimation reduces

1167   simulated carbon sensitivity to climate, Nature Climate Change, 6, 407-411, 10.1038/nclimate2878, 2016.

1168   Spafford, L. and MacDougall, A. H.: Validation of terrestrial biogeochemistry in CMIP6 Earth system models: a

1169   review, Geosci. Model Dev., 14, 5863-5889, 10.5194/gmd-14-5863-2021, 2021.

1170   Sullivan, M. J. P., Lewis, S. L., Affum-Baffoe, K., Castilho, C., Costa, F., Sanchez, A. C., Ewango, C. E. N.,

1171   Hubau, W., Marimon, B., Monteagudo-Mendoza, A., Qie, L., Sonké, B., Martinez, R. V., Baker, T. R., Brienen,

1172   R. J. W., Feldpausch, T. R., Galbraith, D., Gloor, M., Malhi, Y., Aiba, S.-I., Alexiades, M. N., Almeida, E. C., de

1173   Oliveira, E. A., Dávila, E. Á., Loayza, P. A., Andrade, A., Vieira, S. A., Aragão, L. E. O. C., Araujo-Murakami,

1174   A., Arets, E. J. M. M., Arroyo, L., Ashton, P., Aymard C., G., Baccaro, F. B., Banin, L. F., Baraloto, C., Camargo,

1175   P. B., Barlow, J., Barroso, J., Bastin, J.-F., Batterman, S. A., Beeckman, H., Begne, S. K., Bennett, A. C.,

1176   Berenguer, E., Berry, N., Blanc, L., Boeckx, P., Bogaert, J., Bonal, D., Bongers, F., Bradford, M., Brearley, F. Q.,

1177   Brncic, T., Brown, F., Burban, B., Camargo, J. L., Castro, W., Céron, C., Ribeiro, S. C., Moscoso, V. C., Chave,

1178   J., Chezeaux, E., Clark, C. J., de Souza, F. C., Collins, M., Comiskey, J. A., Valverde, F. C., Medina, M. C., da

1179   Costa, L., Dančák, M., Dargie, G. C., Davies, S., Cardozo, N. D., de Haulleville, T., de Medeiros, M. B., del

1180   Aguila Pasquel, J., Derroire, G., Di Fiore, A., Doucet, J.-L., Dourdain, A., Droissart, V., Duque, L. F.,

1181   Ekoungoulou, R., Elias, F., Erwin, T., Esquivel-Muelbert, A., Fauset, S., Ferreira, J., Llampazo, G. F., Foli, E.,
1182   Ford, A., Gilpin, M., Hall, J. S., Hamer, K. C., Hamilton, A. C., Harris, D. J., Hart, T. B., Hédl, R., Herault, B.,
1183   Herrera, R., Higuchi, N., Hladik, A., Coronado, E. H., Huamantupa-Chuquimaco, I., Huasco, W. H., Jeffery, K.
1184   J., Jimenez-Rojas, E., Kalamandeen, M., Djuikouo, M. N. K., Kearsley, E., Umetsu, R. K., Kho, L. K., Killeen,
1185   T., Kitayama, K., Klitgaard, B., Koch, A., Labrière, N., Laurance, W., Laurance, S., Leal, M. E., Levesley, A.,
1186   Lima, A. J. N., Lisingo, J., Lopes, A. P., Lopez-Gonzalez, G., Lovejoy, T., Lovett, J. C., Lowe, R., Magnusson,
1187   W. E., Malumbres-Olarte, J., Manzatto, Â. G., Marimon, B. H., Marshall, A. R., Marthews, T., de Almeida Reis,
1188   S. M., Maycock, C., Melgaço, K., Mendoza, C., Metali, F., Mihindou, V., Milliken, W., Mitchard, E. T. A.,
1189   Morandi, P. S., Mossman, H. L., Nagy, L., Nascimento, H., Neill, D., Nilus, R., Vargas, P. N., Palacios, W.,
1190   Camacho, N. P., Peacock, J., Pendry, C., Peñuela Mora, M. C., Pickavance, G. C., Pipoly, J., Pitman, N., Playfair,
1191   M., Poorter, L., Poulsen, J. R., Poulsen, A. D., Preziosi, R., Prieto, A., Primack, R. B., Ramírez-Angulo, H.,
1192   Reitsma, J., Réjou-Méchain, M., Correa, Z. R., de Sousa, T. R., Bayona, L. R., Roopsind, A., Rudas, A.,
1193   Rutishauser, E., Abu Salim, K., Salomão, R. P., Schietti, J., Sheil, D., Silva, R. C., Espejo, J. S., Valeria, C. S.,
1194   Silveira, M., Simo-Droissart, M., Simon, M. F., Singh, J., Soto Shareva, Y. C., Stahl, C., Stropp, J., Sukri, R.,
1195   Sunderland, T., Svátek, M., Swaine, M. D., Swamy, V., Taedoumg, H., Talbot, J., Taplin, J., Taylor, D., ter Steege,
1196   H., Terborgh, J., Thomas, R., Thomas, S. C., Torres-Lezama, A., Umunay, P., Gamarra, L. V., van der Heijden,
1197   G., van der Hout, P., van der Meer, P., van Nieuwstadt, M., Verbeeck, H., Vernimmen, R., Vicentini, A., Vieira,
1198   I. C. G., Torre, E. V., Vleminckx, J., Vos, V., Wang, O., White, L. J. T., Willcock, S., Woods, J. T., Wortel, V.,
1199   Young, K., Zagt, R., Zemagho, L., Zuidema, P. A., Zwerts, J. A., and Phillips, O. L.: Long-term thermal sensitivity
1200   of Earth's tropical forests, Science, 368, 869-874, 10.1126/science.aaw7578, 2020.

1201   Tramontana, G., Jung, M., Schwalm, C. R., Ichii, K., Camps-Valls, G., Ráduly, B., Reichstein, M., Arain, M. A.,
1202   Cescatti, A., Kiely, G., Merbold, L., Serrano-Ortiz, P., Sickert, S., Wolf, S., and Papale, D.: Predicting carbon
1203   dioxide and energy fluxes across global FLUXNET sites with regression algorithms, Biogeosciences, 13, 4291-
1204   4313, 10.5194/bg-13-4291-2016, 2016.

1205   Vårhammar, A., Wallin, G., McLean, C. M., Dusenge, M. E., Medlyn, B. E., Hasper, T. B., Nsabimana, D., and
1206   Uddling, J.: Photosynthetic temperature responses of tree species in Rwanda: evidence of pronounced negative
1207   effects of high temperature in montane rainforest climax species, New Phytologist, 206, 1000-1012,
1208   https://doi.org/10.1111/nph.13291, 2015.

1209   Walker, A. P., Beckerman, A. P., Gu, L., Kattge, J., Cernusak, L. A., Domingues, T. F., Scales, J. C., Wohlfahrt,
1210   G., Wullschleger, S. D., and Woodward, F. I.: The relationship of leaf photosynthetic traits – Vcmax and Jmax –
1211   to leaf nitrogen, leaf phosphorus, and specific leaf area: a meta-analysis and modeling study, Ecology and
1212   Evolution, 4, 3218-3235, https://doi.org/10.1002/ece3.1173, 2014.

1213   Walker, A. P., Johnson, A. L., Rogers, A., Anderson, J., Bridges, R. A., Fisher, R. A., Lu, D., Ricciuto, D. M.,
1214   Serbin, S. P., and Ye, M.: Multi-hypothesis comparison of Farquhar and Collatz photosynthesis models reveals
1215   the unexpected influence of empirical assumptions at leaf and global scales, Global Change Biology, 27, 804-822,
1216   https://doi.org/10.1111/gcb.15366, 2021.

1217   Way, D. A. and Sage, R. F.: Elevated growth temperatures reduce the carbon gain of black spruce [Picea mariana
1218   (Mill.) B.S.P.], Global Change Biology, 14, 624-636, https://doi.org/10.1111/j.1365-2486.2007.01513.x, 2008.

1219 Way, D. A. and Yamori, W.: Thermal acclimation of photosynthesis: on the importance of adjusting our
1220 definitions and accounting for thermal acclimation of respiration, Photosynthesis Research, 119, 89-100,
1221 10.1007/s11120-013-9873-7, 2014.

1222 Way, D. A., Stinziano, J. R., Berghoff, H., and Oren, R.: How well do growing season dynamics of photosynthetic
1223 capacity correlate with leaf biochemistry and climate fluctuations?, Tree Physiology, 37, 879-888,
1224 10.1093/treephys/tpx086, 2017.

1225 Weedon, G. P., Balsamo, G., Bellouin, N., Gomes, S., Best, M. J., and Viterbo, P.: The WFDEI meteorological
1226 forcing data set: WATCH Forcing Data methodology applied to ERA-Interim reanalysis data, Water Resources
1227 Research, 50, 7505-7514, https://doi.org/10.1002/2014WR015638, 2014.

1228 Williams, K. D., Copsey, D., Blockley, E. W., Bodas-Salcedo, A., Calvert, D., Comer, R., Davis, P., Graham, T.,
1229 Hewitt, H. T., Hill, R., Hyder, P., Ineson, S., Johns, T. C., Keen, A. B., Lee, R. W., Megann, A., Milton, S. F.,
1230 Rae, J. G. L., Roberts, M. J., Scaife, A. A., Schiemann, R., Storkey, D., Thorpe, L., Watterson, I. G., Walters, D.
1231 N., West, A., Wood, R. A., Woollings, T., and Xavier, P. K.: The Met Office Global Coupled Model 3.0 and 3.1
1232 (GC3.0 and GC3.1) Configurations, Journal of Advances in Modeling Earth Systems, 10, 357-380,
1233 https://doi.org/10.1002/2017MS001115, 2018.

1234 Wilson K.B, Baldocchi D.D, and P.J., H.: Leaf age affects the seasonal pattern of photosynthetic capacityand net
1235 ecosystem exchange of carbon in a deciduous forest, Plant, Cell & Environment, 24, 571-583, 2001.

1236 Wiltshire, A. J., Duran Rojas, M. C., Edwards, J. M., Gedney, N., Harper, A. B., Hartley, A. J., Hendry, M. A.,
1237 Robertson, E., and Smout-Day, K.: JULES-GL7: the Global Land configuration of the Joint UK Land
1238 Environment Simulator version 7.0 and 7.2, Geosci. Model Dev., 13, 483-505, 10.5194/gmd-13-483-2020, 2020.

1239 Wohlfahrt, G., Bahn, M., Haubner, E., Horak, I., Michaeler, W., Rottmar, K., Tappeiner, U., and Cernusca, A.:
1240 Inter-specific variation of the biochemical limitation to photosynthesis and related leaf traits of 30 species from
1241 mountain grassland ecosystems under different land use, Plant, Cell & Environment, 22, 1281-1296,
1242 https://doi.org/10.1046/j.1365-3040.1999.00479.x, 1999.

1243 Xiao, Z., Liang, S., Wang, J., Xiang, Y., Zhao, X., and Song, J.: Long-Time-Series Global Land Surface Satellite
1244 Leaf Area Index Product Derived From MODIS and AVHRR Surface Reflectance, IEEE Transactions on
1245 Geoscience and Remote Sensing, 54, 5301-5318, 10.1109/TGRS.2016.2560522, 2016.

1246 Yamaguchi, D. P., Nakaji, T., Hiura, T., and Hikosaka, K.: Effects of seasonal change and experimental warming
1247 on the temperature dependence of photosynthesis in the canopy leaves of Quercus serrata, Tree Physiology, 36,
1248 1283-1295, 10.1093/treephys/tpw021, 2016.

1249 Yamori, W., Hikosaka, K., and Way, D. A.: Temperature response of photosynthesis in C3, C4, and CAM plants:
1250 temperature acclimation and temperature adaptation, Photosynthesis Research, 119, 101-117, 10.1007/s11120-
1251 013-9874-6, 2014.

1252 Zeng, Z., Piao, S., Li, L. Z. X., Zhou, L., Ciais, P., Wang, T., Li, Y., Lian, X., Wood, E. F., Friedlingstein, P.,
1253 Mao, J., Estes, L. D., Myneni, Ranga B., Peng, S., Shi, X., Seneviratne, S. I., and Wang, Y.: Climate mitigation

1254   from vegetation biophysical feedbacks during the past three decades, Nature Climate Change, 7, 432-436,

1255   10.1038/nclimate3299, 2017.

1256   Zhang, X. W., Wang, J. R., Ji, M. F., Milne, R. I., Wang, M. H., Liu, J.-Q., Shi, S., Yang, S.-L., and Zhao, C.-M.:

1257   Higher Thermal Acclimation Potential of Respiration but Not Photosynthesis in Two Alpine Picea Taxa in

1258   Contrast to Two Lowland Congeners, PLOS ONE, 10, e0123248, 10.1371/journal.pone.0123248, 2015.

1259   Zhao, M. and Running, S. W.: Drought-Induced Reduction in Global Terrestrial Net Primary Production from

1260   2000 Through 2009, Science, 329, 940-943, 10.1126/science.1192666, 2010.

1261   Zhao, M., Running, S. W., and Nemani, R. R.: Sensitivity of Moderate Resolution Imaging Spectroradiometer

1262   (MODIS) terrestrial primary production to the accuracy of meteorological reanalyses, Journal of Geophysical

1263   Research: Biogeosciences, 111, https://doi.org/10.1029/2004JG000004, 2006.

1264   Zhao, M., Heinsch, F. A., Nemani, R. R., and Running, S. W.: Improvements of the MODIS terrestrial gross and

1265   net   primary   production   global   data   set,   Remote   Sensing   of   Environment,   95,   164-176,

1266   https://doi.org/10.1016/j.rse.2004.12.011, 2005.

1267   Ziehn, T., Kattge, J., Knorr, W., and Scholze, M.: Improving the predictability of global CO2 assimilation rates

1268   under climate change, Geophysical Research Letters, 38, https://doi.org/10.1029/2011GL047182, 2011.

1269